Flow Turbulence Combust (2014) 92:607–649
DOI 10.1007/s10494-013-9518-0

Thin Shear Layer Structures in High Reynolds Number Turbulence

Tomographic Experiments and a Local Distortion Model

Julian C. R. Hunt · Takashi Ishihara · Nicholas A. Worth · Yukio Kaneda

Received: 30 April 2013 / Accepted: 19 September 2013 / Published online: 22 October 2013

Abstract Three-dimensional tomographic time dependent PIV measurements of high Reynolds number (Re) laboratory turbulence are presented which show the existence of long-lived, highly sheared thin layer eddy structures with thickness of the order of the Taylor microscale and internal fluctuations. Highly sheared layer structures are also observed in direct numerical simulations of homogeneous turbulence at higher values of Re (Ishihara et al., Annu Rev Fluid Mech 41:165–180, 2009). But in the latter simulation, where the fluctuations are more intense, the layer thickness is greater. A rapid distortion model describes the structure and spectra for the velocity fluctuations outside and within 'significant' layers; their spectra are similar to the Kolmogorov (C R Acad Sci URSS 30:299–303, 1941) and Obukhov (Dokl Akad Nauk SSSR 32:22–24, 1941) statistical model (KO) for the whole flow. As larger-scale eddy motions are blocked by the shear layers, they distort smaller-scale eddies leading to local zones of down-scale and up-scale transfer of energy. Thence the energy spectrum for high wave number k is $E_X(k) \sim Bk^{-2p}$. The exponent p depends on the forms of the large eddies. The non-linear interactions between the distorted inhomogeneous eddies produce a steady local structure, which implies that $2p = 5/3$ and a

J. C. R. Hunt
Department of Earth Sciences, University College London, London WC1E 6BT, UK

J. C. R. Hunt
Trinity College, Cambridge, CB2 1TQ, UK

T. Ishihara (✉)
Graduate School of Engineering, Nagoya University, Nagoya 464-8603, Japan
e-mail: ishihara@cse.nagoya-u.ac.jp

N. A. Worth
Department of Engineering, University of Cambridge, Trumpington Street, Cambridge, CB2 1PZ, UK

Y. Kaneda
Center for General Education, Aichi Institute of Technology, Toyota 470-0392, Japan

flux of energy into the thin-layers balancing the intense dissipation, which is much greater than the mean $\langle\epsilon\rangle$. Thence $B \sim \langle\epsilon\rangle^{2/3}$ as in KO. Within the thin layers the inward flux energises extended vortices whose thickness and spacing are comparable with the viscous microscale. Although peak values of vorticity and velocity of these vortices greatly exceed those based on the KO scaling, the form of the viscous range spectrum is consistent with their model.

Keywords High Reynolds number turbulence · Intermittency · Thin shear layers · Tomographic experiments · Local distortion model

1 Introduction

Numerical simulations of homogeneous turbulence at very high Reynolds number (of the order of 1000 based on the Taylor microscale), reviewed by Ishihara, Gotoh and Kaneda (IGK) [1], were used in the preceding paper (referred to as IKH—see [2]) to analyse the general form and detailed statistics of the flow near and within the 'significant' thin layer structures. These are identified as where the average vorticity in the structure is much greater than the rms vorticity. Typically they are sheared with an average velocity 'jump' across them of the order of the rms velocity of the turbulence (u_o). But in these computational studies it was not practical, given the amount of spatial data, to track such structures with time.

In Section 2 of this follow-up paper laboratory experiments are conducted in a turbulent flow driven by oppositely rotating discs at high enough Reynolds numbers (Re) to study the unsteady structure of eddy motions down to scales comparable with the Kolmogorov microscale. In the central region between the discs the turbulence is approximately homogeneous. Turbulent flows in this kind of experimental apparatus have been studied before (e.g. [5–7]), but the 2 m high apparatus used here enables a very wide range of scales (of order of 1000) to be measured and visualized with a three-dimensional time varying digital PIV system, whose measuring volume is large enough to observe how the structures move and distort with time. In order to ensure the generality of the results small scale velocity statistics were measured and compared with those in other homogeneous and inhomogeneous experiments.

The layers studied here are similar to those that occur outside turbulent shear layers, such as jets and wakes [8]. But in these interior thin-shear layers significant levels of turbulent energy exist on both sides of the layer, leading to small-scale motions entering the layers. Such thin layers also occur in rapidly developing turbulence in the near wakes of bluff bodies, whose spectra are quite similar to that of fully developed turbulence [9]. Extensive analysis of conditional sampling of the velocity fields relative to the location of the thin layers have been performed for experimental flows by Westerweel et al. [8] and in direct simulations [10], which enabled the conditional one point and two point moments to be studied inside and outside the thin layers. The same level of conditional analysis has not yet been performed for thin layers within turbulent flow regions. Previous studies of the dominant coherent structures in homogeneous turbulence have been at lower Reynolds numbers and came to different conclusions, namely that the dominant structures are elongated vortices, some of which may merge [11, 12]. Flat thin structures soon break up into Kelvin Helmholtz instabilities in such flows (e.g. [13]). But in the turbulent flow

studied here at higher Reynolds number ($160 < R_\lambda < 500$) the turbulence integral scale is much larger than the Taylor microscale, so that external eddy motions inhibit such instabilities and maintains the shear layers [14, 15]. The level of small scale fluctuations within the layers depends on R_λ, so that the internal structure and thickness of the experimental thin layers described here differ from the numerical simulations of IKH at even higher $R_\lambda (> 1000)$.

In Section 3 of this paper we derive from local kinematic and dynamical models, the spatial Fourier description and physical scaling of typical eddies and velocity fluctuations outside and within the significant thin layers. Thence we derive their statistics in local and in fixed coordinates. This analysis, based on previous studies of interactions between large and small fluctuating flow fields (e.g. [16–18]), is applied to how external eddies larger than the layer thickness are 'blocked' as they impact on the thin shear layer [19, 20]. The mechanism whereby such layers remain sharp was analysed by Hunt et al. [15]. The straining associated with the impacting (and separating) motions of large eddies distorts smaller scales sufficiently strongly that the linearized inhomogeneous 'rapid distortion theory' of Hunt [21] is valid. It is generalized here to derive, first, the local Fourier transforms over the spacing L_S between such layers, where L_S is the order of the integral length scale L, and then, using the method of stationary phase, a general asymptotic form of the spatially averaged spectrum $E_X^{(lin)}(k)$ proportional to k^{-2p} for the small scale eddies for $kL \gg 1$, in terms of the large scale straining, but independently of the small scale eddies' arbitrary unknown spectra.

Following Obukhov [4] and Townsend [16], (OT)'s model of non-linear transfer of energy between larger and smaller scales is applied to this spectrum of semi-organised inhomogeneous eddy motion. Based on the observation that the local turbulence structure is in local equilibrium, the OT model leads to a unique form of self similar inertial range spectrum $E_X^{(non-lin)}(k) \sim k^{-2p}$, with the value of $2p = 5/3$, as discovered by Kolmogorov [3] and Obukhov [4] (KO). This corresponds to a dynamically stable distribution of eddies, whereas other kinds of groups or forms of eddies, whose spectra have different values of $2p$, either grow or decay.

In this locally inhomogeneous situation the net transfer of energy towards the smallest scale eddies near the interface causes a net flux F_ℓ of energy into the thin layers. This determines the magnitude of the external 'inertial range' turbulence and the very high dissipation rate in the thin layer which greatly exceeds that in the exterior region. By considering the whole energy balance between the turbulence inside and outside the thin layer, the 'inertial range' energy spectrum outside the layer $E(k)$ can be expressed in terms of the average dissipation rate $\langle \epsilon \rangle$ over the whole flow. This is consistent with KO theory. Thus in this region for a characteristic equilibrium statistical structure tends to form quite fast. This conceptual structure differs from those where particular types of eddy dominate the flow structure, such as the quasi-steady spiral vortex mechanisms proposed by Lundgren [22] and Horiuti and Ozawa [23], which also imply a specific value of $2p$.

The visco-inertial dynamics of the fluctuations within the thin layers triggered by the external eddies are estimated using locally linear concepts. This leads to typical magnitudes for the peak vorticity and velocity of the elongated microscale eddies, which are shown to be much greater than those estimated from the KO model. These determine the raised values of the peak and average values of the dissipation rate in the significant thin layers.

This paper does not focus on the weaker and smaller isolated structures, such as weak vortices and streaks, that exist between the significant thin layers, and which largely determine the average second and third order moments. Because of their random intermittent distribution in space and time (e.g. [24, 25]), it is likely that the overall spectrum is determined by the spectra of these individual structures. Also semi organized dynamics in these weaker structures are similar in some respects to those near thin layers. So the detailed study of this paper may provide a basis for describing the whole flow field.

Our ideas about the effects of the significant shear layers on the dynamics and kinematics have been derived from many previous studies. Observations of large, almost discontinuous velocities have been noted previously as being inconsistent with a smooth distribution of eddy motions decreasing in strength as their size decreases [26–28]. The consequences for turbulence eddy structure were discussed by R. Betchov and H. Liepmann at the famous conference on turbulence at Marseille (CNRS 1962), when they argued that experiments and theory were needed to develop a model of turbulence that accounted for the formation and dynamics of thin intermittent regions with high dissipation and shear (see also [29]). Later experiments and analysis [30, 31] have shown that sharp continuous interfaces occur at the edges of turbulent regions, with high vorticity and significant impacts on the nearby velocity and scalar fluctuations [8, 15]. IGK were the first to show that they also occur widely within turbulent flows at high Reynolds number.

Many experiments and analyses have described turbulent flows in terms of evolving and interacting coherent structures and how they are distributed, in terms of Eulerian and/or conditional statistics (e.g. [32–34]), and contrasted this with representation in terms of distributions of standard functions, such as Fourier series [35].

In the model developed here the moments and spectra are also determined by the ensemble of flow structures of a particular type, which in this case are thin shear layers with internal smaller scale vortices. The analysis of the simulations in IKH shows that the significant thin layers are neither highly curved, nor space filling. This observation is used in the scaling analysis and modeling of the layers.

Some previous studies of coherent structures have indicated how they affect the transfer of energy between different scales of eddy motion, whether upwards or downwards or both. Energy transfer mechanisms between large and small scale eddy motions can be examined in physical space by analysing the vorticity dynamics of individual eddy structures within straining regions and their statistical ensembles (e.g. [16, 29, 35]). This approach enables the significant upscale transfer of energy to be modeled which is not included in the statistical physics approach developed by Kraichnan [36] and others. The implications for scalar fluctuations of interactions between different scales and coherent patterns of scalars were simulated and analysed by considering three point moments [37]. Numerical simulations based on Eulerian analyses of the dynamics of the Fourier components of homogeneous turbulence (e.g. [38, 39]) have shown that the maximum net energy transfer is primarily caused by interactions between eddies which are just larger and just smaller than each other. This is consistent with the Richardson and KO statistical cascade concept. Previous simulations of three-dimensional turbulence have shown that upscale energy transfer is comparable to downscale, though the latter is on average larger (IGK). Aoyama et al. [40] showed that there are separate, but adjacent zones (on scales comparable with the integral scale L) where the energy transfer is predominantly upwards or downwards. The modeling of Section 3 shows that this transfer is associated with

inhomogeneity of the different scales of turbulence near the interface, which has not been noted in previous studies based on the usual statistical analysis.

The conditional data and new analysis given in IKH provides methods for studying non-ideal aspects of high Reynolds number turbulence. When eddies have significant helicity, both up and down scale transfer are reduced [41]. One of the reasons why KO theory has been so useful for describing the statistical structure of the small scales of turbulence is that, although it is an equilibrium theory, it applies even when the overall flows is quite inhomogeneous and far from equilibrium (e.g. [42]). But the limitations of this approximation need more investigation. Also certain aspects corresponding to the KO statistics, e.g. second order spectrum, are observed experimentally when other aspects, such isotropy and higher order spectra, are inconsistent with the theory [43]. The new model presented here and the simulations of the fluxes of energy (IKH), help explain the important property of turbulence that it adjusts much faster in space and time than is predicted by the slow, down-scale cascade model of Richardson and KO.

2 Tomographic PIV Measurements of Significant Structures

2.1 Experimental apparatus and calibration

In a number of previous experiments, fine scale turbulent structures have been measured in the flow between two counter-rotating disks or impellers (see e.g. [5–7, 44, 45]). The apparatus in the Cambridge University Engineering Department is a large 2m diameter dodecahedral perspex water mixing tank, as shown in Fig. 1. Note xyz coordinates (with x horizontal and parallel to laser and y vertical).

Two eight vane 0.8 m diameter impellers, at a separation distance of 1.25 m are counter-rotated causing the fluid nearest the impellers to spin in opposite directions, establishing a strong shear plane in the centre of the tank. Two secondary toroidal recirculation regions are formed, which stretches the flow in the central region. Radial baffles were fitted on the outside wall to remove any net rotation, and further increase turbulence production. The Reynolds number based on impeller radius, R_I, and rate of rotation, Ω_I, is $Re = \Omega_I R_I^2/\nu$ which ranged from 4×10^4 to 3×10^5. The apparatus achieves its two main objectives of generating high Reynolds numbers turbulence with constant energy injection at the largest scales; and secondly a closed

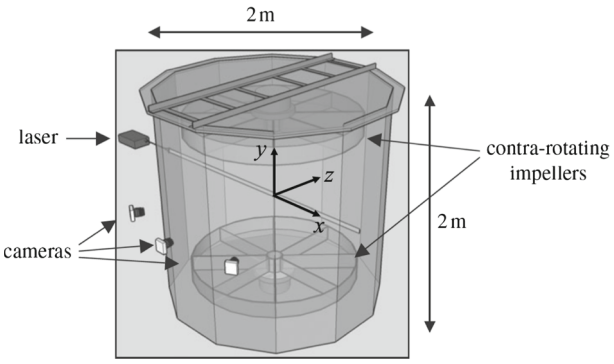

Fig. 1 Schematic diagram of the experimental apparatus

geometry which permits the spatial evolution of flow structures to be studied within the measuring volume before being transported away by the mean flow.

Here, the size of the tank is such that the Kolmogorov micro-length scales ($\eta = (\nu^3/\langle\epsilon\rangle)^{1/4}$) and time scales ($\tau = (\nu/\langle\epsilon\rangle)^{1/2}$) are large enough to be approximately resolved with the PIV measuring techniques. A total of four PIV experiments were conducted at different resolutions to characterise the flow and assess spatial resolution limitations. For brevity only two of these are presented in this paper, denoted as cases D1 and D4. A single Tomographic PIV case was conducted, denoted as case T1. For full details of the PIV setup, camera calibration, tomographic reconstruction, and cross-correlation algorithms the reader is referred to [46].

Before investigating the nature of the fine scale flow structures it is necessary to characterise the flow in terms of both statistical turbulent properties and typical length and time scales, over the range of Reynolds number of the experiments.

Some typical flow properties are listed in Table 1. Since measurements were confined to a central volume the average rate of dissipation, $\langle\epsilon\rangle$, had to be estimated using a scaling argument method (defined as $\langle\epsilon\rangle = Au^3/\Lambda$ using a constant value of $A = 0.5$, [47], and a value of the integral length scale $\Lambda = 130$ mm estimated from the velocity correlation function). These values agree with estimates using other methods [48]. This enabled the Kolmogorov microscale, η, and Taylor microscale λ to be calculated. For $R_\lambda = 162$, $\lambda/\eta \sim 25$, and for $R_\lambda = 458$, $\lambda/\eta \sim 42$. Thus there are large separations of scales so that high Reynolds number processes could be studied.

The relative spatial resolution is defined as the interrogation window size h normalized by η, i.e. h/η. The 50 % window overlap gives a vector spacing, $\Delta x/\eta$, of half this value. With increasing Reynolds number, there is a reduction in resolution. However, for the lower Reynolds number runs in the D4 and T1 cases, a resolution $\Delta x/\eta \sim 3$ is achieved, which as discussed in [46], means that, since $\Delta x/\lambda < 4$, the flow structures and the internal fluctuations are approximately resolved.

Because of the high value of the Reynolds number, the rms velocity is found to increase linearly with the impeller rotation frequency, and is about 30 % of the peak swirl velocity.

Table 1 Experimental properties

Case	$\Omega_I R_I$ (mm/s)	Re	R_λ	$u_{\rm rms}$ (mm/s)	η (mm)	$\langle\epsilon\rangle$ (m^2/s^3)	τ (ms)	$\nu \times 10^6$ (m^2/s)	x/η	h/η
D1-1	56.0	3.77×10^4	240	17.4	0.536	2.01×10^{-5}	243	1.18	6.71	13.4
D1-2	112	7.55×10^4	334	33.6	0.327	1.45×10^{-4}	90.5	1.18	11.0	22.0
D1-3	223	1.51×10^5	479	69.1	0.191	1.26×10^{-3}	30.7	1.18	18.9	37.8
D1-4	335	2.26×10^5	581	102	0.143	4.01×10^{-3}	17.2	1.18	25.2	50.4
D1-5	447	2.94×10^5	651	131	0.120	8.67×10^{-3}	11.8	1.22	30.0	60.0
D4-1	112	8.06×10^4	335	31.7	0.326	1.21×10^{-4}	95.6	1.11	1.67	3.34
D4-2	223	1.61×10^5	501	70.8	0.178	1.36×10^{-3}	28.6	1.11	3.05	6.10
D4-3	335	2.42×10^5	548	84.7	0.156	2.32×10^{-3}	21.9	1.11	3.49	6.98
D4-4	447	3.22×10^5	700	138	0.108	1.01×10^{-2}	10.5	1.11	5.04	10.1
T1-1	28.0	1.86×10^4	162	7.98	0.972	1.94×10^{-6}	787	1.20	1.09	2.18
T1-2	56.0	3.72×10^4	224	15.3	0.595	1.38×10^{-5}	295	1.20	1.79	3.58
T1-3	112	7.45×10^4	323	31.8	0.344	1.23×10^{-4}	98.7	1.20	3.10	6.20
T1-4	223	1.49×10^5	458	64.1	0.204	1.00×10^{-3}	34.6	1.20	5.24	10.5
T1-5	335	2.23×10^5	555	94.1	0.153	3.18×10^{-3}	19.4	1.20	6.99	14.0

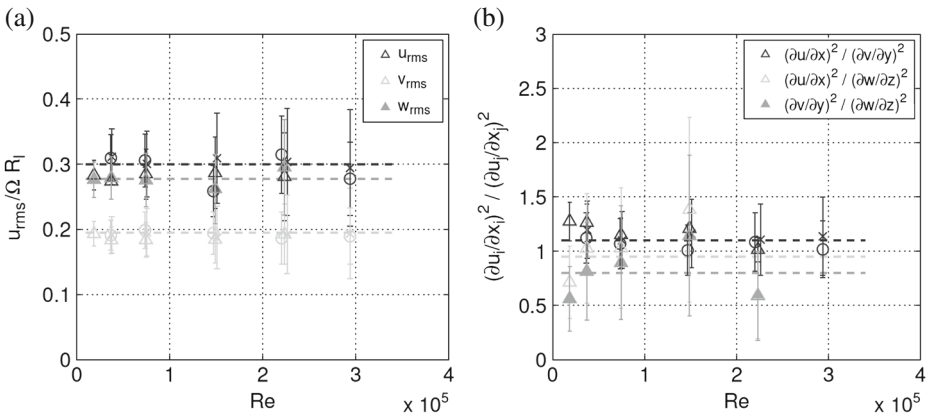

Fig. 2 **a** rms velocity ratios and **b** Velocity gradient ratio. Components by colour and fill colour as indicated, case by symbol:×, D1; ◯, D4; △, T1; – – –, mean component value averaged over all cases and runs

Figure 2a shows that the turbulence structure between the rotors is anisotropic, but the anisotropy does not vary with the Reynolds number. The ratio of radial and axial velocity components is ∼1.5, which agrees well with values in other experiments (e.g. [6]). However at the smallest scales the turbulence is approximately statistically isotropic to the extent as seen by the isotropy of the mean squared velocity gradients, shown in Fig. 2b. However there is some degree of scatter because the eddy motions at the microscales are not fully resolved.

To test whether the small-scale flow structure was statistically the same as in other high *Re* flows, including those with large-scale anisotropy, the two-point longitudinal structure function Δu^2 was measured and compared with the well established Kolmogorov's [3] two-thirds law, plotted (for the D1 case) logarithmically in Fig. 3. The results agree approximately with those of previous experiments when the spacing is a fraction of the integral scale i.e. where $r \sim (1/3)\Lambda$ [49, 50].

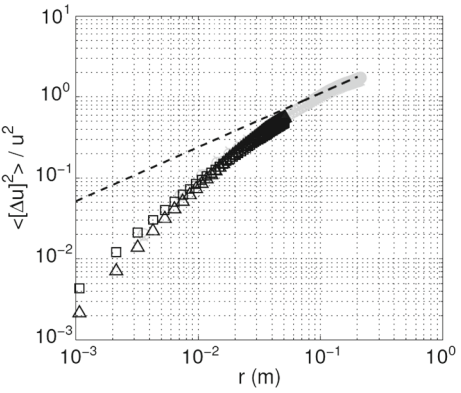

Fig. 3 Longitudinal second order structure function. *Colours* representing cases: T1, *black*; D1, *grey*. *Symbols* representing run number: ×, D1-1; ◯, D1-5; △, T1-1; □, T1-5; – – –, $\langle[\Delta u]^2\rangle/u^2 = C_2\langle\langle\epsilon\rangle r\rangle^{2/3}/u^2$

2.2 Study of coherent structures

Having characterised the Reynolds number scaling and nature of the statistically steady flow, and demonstrated the consistency of the PIV data, the latter will now be used to investigate the Taylor-scale coherent flow structures. In this paper only a few sample structures have been analysed. More detailed statistics are in [48].

In the present investigation coherent structures are defined as continuously connected regions where the enstrophy, Ω, is greater than the rms value, $\Omega > \Omega_{\rm rms}$. Enstrophy is defined here as $\Omega = (1/2)\boldsymbol{\omega} \cdot \boldsymbol{\omega}$ using local vorticity $\boldsymbol{\omega}$. In Fig. 4 not only the regions of high enstrophy but also the regions of low enstrophy are shown. Note that where the vorticity is less intense it is also distributed in isolated patches. These are small scale, but typically bigger than the Kolmogorov microscale. See Fig. 4.

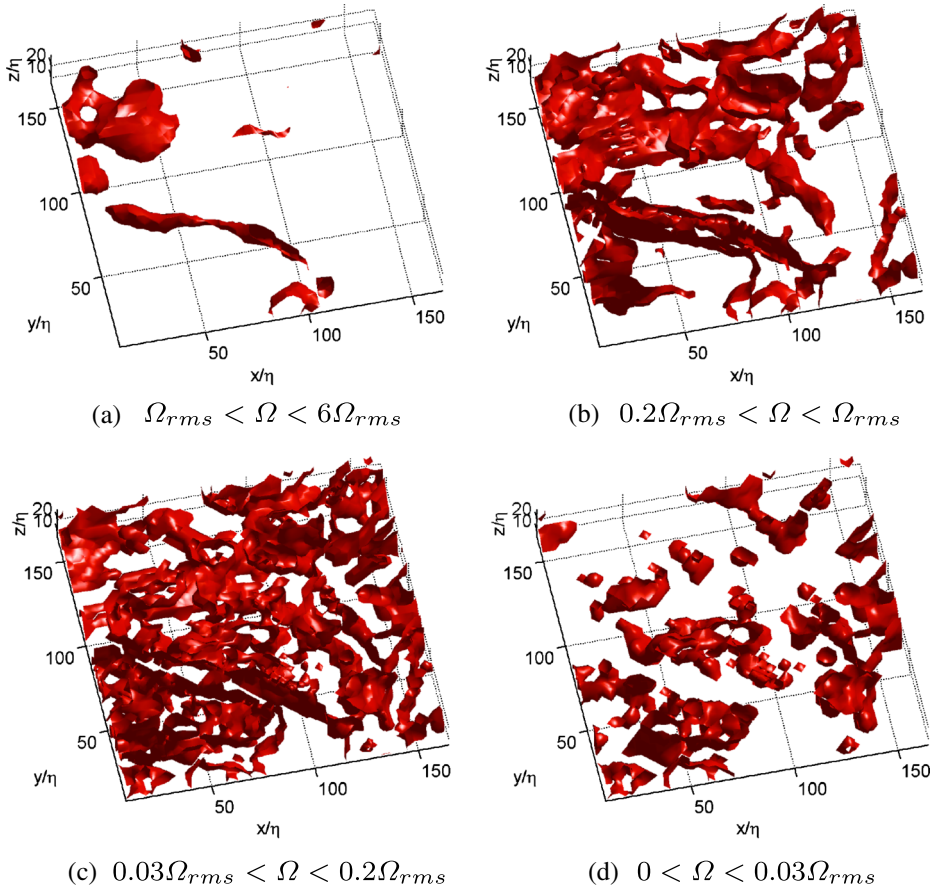

Fig. 4 Isosurfaces of enstrophy for a range of threshold levels (from [48]) showing that the most vorticity fluctuations (greater than rms value) occur in large isolated structures, while weaker fluctuations occur in smaller scale patches that are isolated from each other and that are distributed approximately uniformly

To analyse a range of coherent structures, examples were selected at different Reynolds numbers and shown in Movies 1, 2 and Fig. 5. Iso-surfaces of enstrophy and dissipation rate across a range of coherent threshold values are plotted across a range of threshold levels, $n\times$(mean value), with the colour indicating the level n. To aid viewing, the threshold level is increased, allowing a range of iso-surface levels to be compared on the same plot. The enstrophy and dissipation rate use variable grey tones to show the distribution of different levels of enstrophy and dissipation. A number of shapes can be identified from Fig. 5 with a predominance of short tube-like and ribbon-like structures for both enstrophy and dissipation. The diameter and

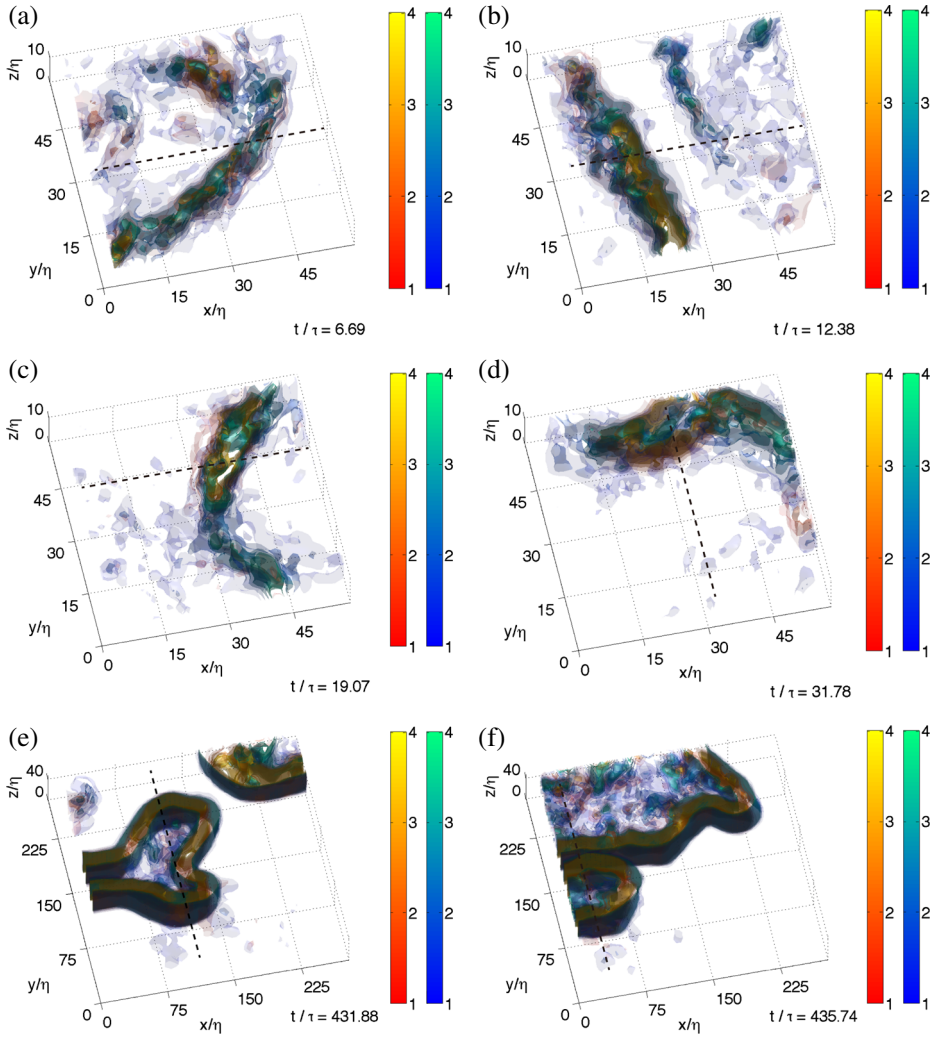

Fig. 5 The three-dimensional structure of thin shear layers. Dissipation (*blue-green*) and enstrophy (*red-yellow*) iso-surfaces. Threshold values are set to $n\times$ ("mean value") ($n = 1, 2, 3, 4$). **a**–**d** $R_\lambda = 162$, $\lambda/\eta = 25$, $t/\tau = 6.69, 12.38, 19.07, 31.78$; **e**, **f** $R_\lambda = 458$, $\lambda/\eta = 42$, $t/\tau = 431.9, 435.7$

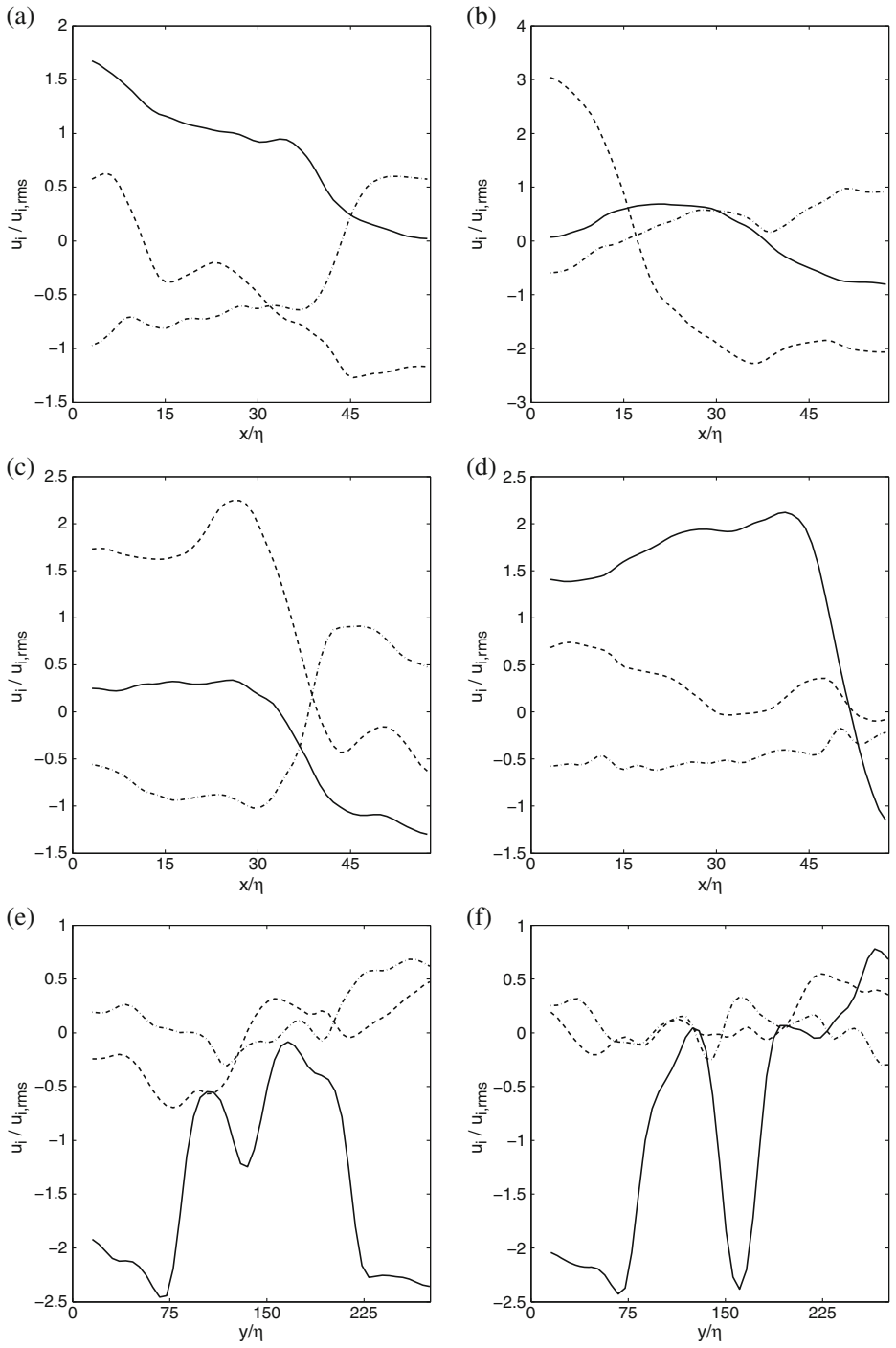
(a)
(b)
(c)
(d)
(e)
(f)
u_i / u_i,rms
x/η
y/η

thickness of these range between 2 to 20 grid points. The results in Fig. 6 show that the velocity differences across the significant layers are comparable with the rms velocity fluctuation for the whole flow region.

A time series of the three-dimensional measurements of the structures in case T1-1 from $t/\tau = 0$ to 41.8 are shown in Movie 1 (Online Resource 1). Here 41.8τ corresponds to $10.8\lambda/u_{\rm rms}$. (See Table 1.) Movie 1 shows that the lifetime of high shear region is enough longer than characteristic time-scale of deformation of the region. The first four images in Fig. 5 are from Movie 1 and have been chosen to illustrate the nature of the thin shear-layer regions. The Reynolds number for this case is $R_\lambda = 162$. A time series of the flow in case T1-4 (a higher Reynolds number case; $R_\lambda = 458$) from $t/\tau = 0$ to 964 are shown in Movie 2 (Online Resource 2). The last two in Fig. 5 are from Movie 2. Here 964τ corresponds to about $250(\lambda/u_{\rm rms})$. Note that fluctuations within the structures are visible for the low *Re* case, but not for the high *Re* case—see below.

The ribbon-like structures are defined using around 4 to 51 grid points (up to the maximum domain size). Accounting for spatial resolution reduction at high Reynolds numbers indicates that the thickness variations vary between 2η to 140η, and their greatest lengths are as much as 360η. The wrinkled surface of the majority of the structures may be caused by large and small-scale deformations.

In example fields selected in the analysis of this section the majority of structures appear to be oriented in the z-direction (see Figs. 1, 4 and 5). Note that the data used in Fig. 2 include not only those in Figs. 4 and 5 but also those for the other cases, which may be less anisotropic than the former. Note also that the smaller volume size in the z-direction severely truncates structures exceeding this size. For example, if tube-like structures are aligned with the z-direction their length will be shortened, but if these are aligned in one of the other two directions they may look ribbon-like structures (i.e. with very different breadths and lengths) or sheet-like structures (with breadths comparable to lengths).

A few simple observations can be made immediately. The regions occupied by the significant structures shown are very long in comparison with their thickness. Although these measurements only show a thick 'slice', and so we cannot know their extent beyond the measurement volume, they appear to extend unchanged through the volume and hence it is, at least, plausible that their third dimension is also large in comparison with the thickness (it seems rather unlikely that the tubes of enstrophy terminate very quickly or change direction very suddenly outside the region of interest). Hence they appear to be 'ribbon like'. More detailed plots combining enstrophy and dissipation [48] show that they consist of sheets of high dissipation rate with embedded vortex structures. A dynamical argument favouring sheets/ribbons is that these structures persist even in the presence of significant fluctuations outside and right across their interiors. The data shows stretching and compression evident in different parts of the shear layers. By contrast interior fluctuations tend to disrupt typical axisymmetric vortices (e.g. [52, 53]).

◀ **Fig. 6** Change in velocity components across the thin shear-layer regions. The three instantaneous velocity components, normalized by their rms values, are shown as they vary along a line marked on Fig. 5. The components are u_1 (x-direction), *solid line*; u_2 (y-direction), *dashed line*; u_3 (z-direction), *dasheddotted line* (from [51])

The thickness of the structures can be estimated from these and other images as about $10-12\eta$ for the low Reynolds number case. This corresponds to approximately 0.5λ, where λ is the Taylor microscale. For the higher Reynolds number case, the thickness is about $20-25\eta$, i.e. again about 0.5λ.

The advection term confirms the direction of movement of the structures. Video sequences (as in Fig. 5) show that as the sheets are advected by the turbulence the structures maintain their overall shear-layer structure as they advect through the volume, although there are occasions when they become more convoluted. Their longevity is consistent with the low values of the enstrophy dissipation outside the layers. Figure 6 shows the change in the three instantaneous velocity components along a line through the shear layer. The line along which this is examined is shown in the previous figures for each case. The instantaneous velocities have been normalized by the rms value of that component for the whole flow. In all cases there are large velocity jumps across the shear layers with magnitudes of approximately two to three times the rms velocity.

Therefore given the thickness of the layers discussed earlier, very large gradients occur across these regions. These scale with the rms velocity divided by the Taylor microscale. Also, the dissipation rate must also scale with these values, which is consistent with the usual definition of the Taylor microscale. Note that the ratio of the global rms velocity to the Kolmogorov microscale velocity is about 6 and 11 in the low and high Reynolds number cases respectively. The appropriate scale for the velocity jumps is indeed the rms velocity rather than the Kolmogorov velocity, since the jump is very large in terms of the Kolmogorov velocity and also the two Reynolds number cases show approximately the same jump in terms of the rms velocity. If scaled with the Kolmogorov velocity there would be a factor of 2 difference. The unusual shapes of the velocity trace in the higher Reynolds number case ((e) and (f)) is because they are derived from measurements taken on cross sectional lines cut through more than one sheet. In the case of (e) the vorticity of the sheets is of opposite sign (though that is not apparent from the enstrophy). As such, the velocity jump across the first sheet is offset by that through the second, leading to no net jump across the pair through a region of high velocity exists between them. In the last case there are two sheets of the same sign leading to an increase, a drop and then another increase, giving an overall jump for the pair.

3 A Model for Thin Shear Layer Structures and High Reynolds Number Turbulence Statistics

3.1 Concepts and theoretical mechanisms

Here a new model is developed for the quasi-universal small scale motions associated with significant thin shear layers in high Re turbulence whose sizes vary between those strongly affected by viscous stresses on the microscale ℓ_v, to those that are dominated by large-scale inertial forces on the energy containing scale L, as shown in IKH and Section 2.2. The average separation distance of these non-overlapping, thin layer structures is L_S, which is of the order of the smallest energy input scale L. (Larger scales of energy input exist in most environmental and geophysical flows. See Figs. 7, 8 and Section 3.4.)

There is no evidence that there is a 'fractal' distribution of these structures (e.g. [54]), as occurs in many other intermittent dissipative processes. But between the significant structures there is a random distribution of moderate to low amplitude disturbances on all scales less than L, whose peak values of vorticity and small-scale velocity are much less than those in the thin shear layers. The dissipation rate is also randomly distributed over all these scales, but does not have the extreme intermittent values found in the significant thin layers, as shown in IKH and Section 2.2.

The significant structures have a characteristic, persistent and common form for the local velocity and scalar distribution, which may be described qualitatively (e.g. in terms of the form of their boundary or of a dominant instability mode) or quantitatively, by defining profiles relative to some part or point in the structure as it moves through the flow, such as the 'edge' of a thin layer (e.g. [10]) or the centre of a vortex. By definition, if the structures are broadly repeatable the quantities can be defined statistically and can be analysed dynamically. This approach differs from the usual statistical and dynamical analysis of turbulence, where the variables are described in terms of idealized (e.g. Fourier, trigonometrical, step functions etc.) or empirical functions that are overlapping (usually space filling) which are defined in fixed or uniformly moving frames (e.g. [32, 55]). However, these classical analytical methods can be applied locally in the frame of moving structures, as we show here. Many previous models of turbulence (e.g. [22]) are based on the same methodology; but their choice

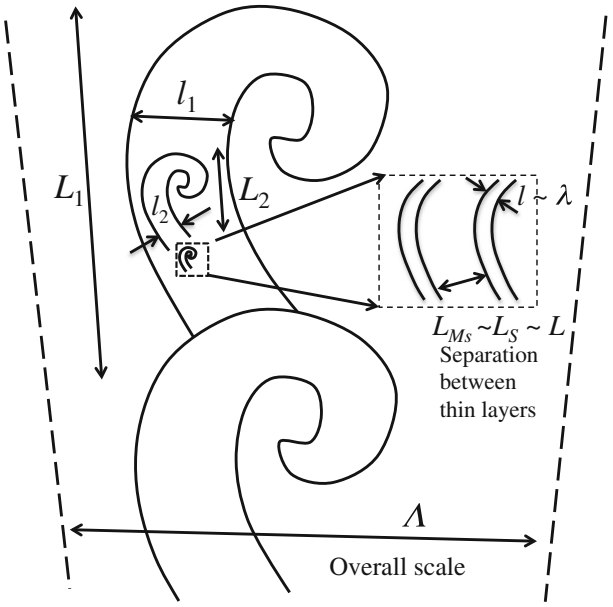

Fig. 7 Typical distribution of different types and scales of large eddy structures in turbulent flows corresponding to different types of forcing or boundary conditions on large scale instability. Each type has scale L_m ($1 \le m \le M_s$) ranging from macroscales $\Lambda \sim L_1$ to the scale of the separation $L_S(= L_{M_s})$ between the thin shear layers with thickness ℓ defines the largest inertial scale eddies (note M_s ranges from 1 in typical homogeneous laboratory flows to ~2 in shear flows, to 3–5 in geophysical flows and greater in astrophysical flows). Note that ℓ is of the order of the Taylor microscale, $\lambda \sim Re^{-1/2} L$, where Re is the Reynolds number of the eddies of scale L

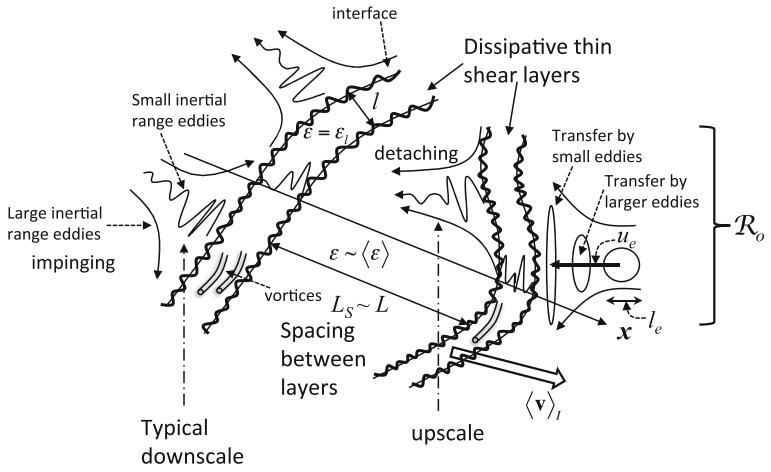

Fig. 8 Characteristic structure and length scales of the inertial range eddy motion in the outside region $\mathcal{R}_o$ adjacent to the thin shear layers showing downscale and upscale eddy distortion mechanisms. The non-linear interactions and distortions of these eddies lead to a net downscale transfer by eddies smaller than k^{-1}. This determines the local equilibrium spectrum of eddies. Note that the layers are moving at a velocity $\langle \mathbf{v} \rangle_l$ averaged across the layer. The small scale energy transferred into the layers is dissipated through the generation of intense elongated microscale vortices—'a spaghetti-sandwich' picture of turbulence

of characteristic model does not correspond to thin layer structures observed in the DNS at very high Re (IKH).

The flow fields observed and measured in the numerical simulations of IKH, and in the laboratory experiments of Section 2, show that thin shear layers form in high Reynolds number turbulence, with a significant velocity jump across them. The laboratory experiments show that they have a repeatable and persistent statistical structure within and outside them. Their thickness ℓ is much less than L_S. Typically the velocity jump across the layer Δu is of order u_o $(= u_{\rm rms})$. On the scale of their thickness ℓ the layers are approximately flat, although they have significant curvature where they roll up at the ends of the layers. Although they move and change their shape, this basic structure persists over a time scale large compared with the Taylor microscale time scale that is of order ℓ/u_o (see Section 2.2).

Other characteristic structures also exist over these scales, such as billows or rolled-up thin shear layers [22, 23]. Models of strain theory [56] and the measurements presented here indicate that these can form at the edges of thin shear layers. But on the evidence presented in IKH and in Section 2, there is no wide spread rolling up of the significant thin layers into spiral vortices with a number of turns sufficient to affect the dynamics or the spectra [57].

Within high Reynolds number turbulent flows small-scale structures are formed by internal dynamics, and/or resistive boundaries and/or body forces [32]. Because the time scales of large eddy structures (away from boundaries) T_L tends to be larger than or comparable with the time over which the flow develops (T_D) [58, 59], the large scales of turbulence are always affected by their initial or boundary conditions.

Therefore they cannot have a completely universal structure, even asymptotically (despite the suggestion in [60]).

However there are well-identified mechanisms that lead to small scales having a number of common forms, despite the different and persistent forms of large-scale eddy structures. As Betchov [61] and subsequent authors have suggested [29, 37], this arises because large scale straining motions in general deform the vorticity of small scale eddy motions, which becomes amplified and concentrated in elongated tubes and extended sheets. However Betchov and others did not emphasize or explain that the most significant sheets are also shear layers, i.e. having vorticity mostly of one sign. Studies of isolated turbulent structures show that unless there is a finite mean value of the vorticity in such structures, they cannot persist and therefore only have a small effect on the flow [62]. As Batchelor and Townsend [63] first proposed, there might be a self-replicating pattern of vertical sheets with energy dissipation concentrated in the sheets. These are effectively thin shear layers because the integrated vorticity in the sheet is finite and varies slowly along the layers. But there has not, until now, been clear experimental evidence that the shear layers tend to be thicker and much wider than the diameters of the most intense vortex tubes in the flow. The fact that the most intense tubes are generally positioned within the layers has not previously been established computationally or explained.

What is the reason for the persistence of vortical layers in high Reynolds number turbulence? Since the vortical layers block or filter external fluctuations [19], they also distort and amplify smaller scale eddies near the layer. The blocking also strengthens the mean shear of the layer and therefore contributes to their persistence [15]. By contrast when individual vortex tubes with diameter ℓ are generated a region with high amplitude, randomly oriented fluctuations, e.g. outside the thin layers, they only interact with these fluctuation over a distance of order ℓ unlike sheet structures which affect the flow over a distance L in general. Also as they distort and amplify external eddies; they also trigger waves within the vortex, which leads to their destruction [52, 64]. In high Reynolds number flow such vortices can only persist if they are shielded from small-scale fluctuations, as occurs within the viscous-inertial thin layers, described in IKH and in Section 3.3.

Because of the high value of Re, the dynamics is assumed to be effectively inviscid in $\mathcal{R}_o$ outside the significant thin shear layers, where eddy structures with scale L impact and depart from the layers (see Fig. 8). Note that the layers, and the regions $\mathcal{R}_o$ are moving through the flow at a local velocity $\langle v \rangle_I$. Straining by larger scale eddies distort smaller eddies (with length scales ℓ_e and velocity u_e significantly less than Δu), as they impact on the shear layer are similar to the distortion of eddies approaching a bluff body [65]. The dominant eddy motion and thence the form of the spatial energy spectrum near the interface is derived from [21] using an asymptotic analysis of the Fourier transform taken across the domain $\mathcal{R}_o$.

Essentially a vortex sheet or thin shear layer acts like a solid plane for weak fluctuations that travel outside the layer at the same speed as the mean flow (e.g. [19, 66]). When a large eddy is being transported and impinges on the plane surface, it is distorted in a similar way to eddies being advected onto a bluff body [20]. Experiments with vortex rings by for example Chu and Falco [67] demonstrate the mechanism.

Near the interface, the small scale amplified eddies interact non-linearly, which amplifies the small-scale turbulence near the interface, e.g. as in the experiments

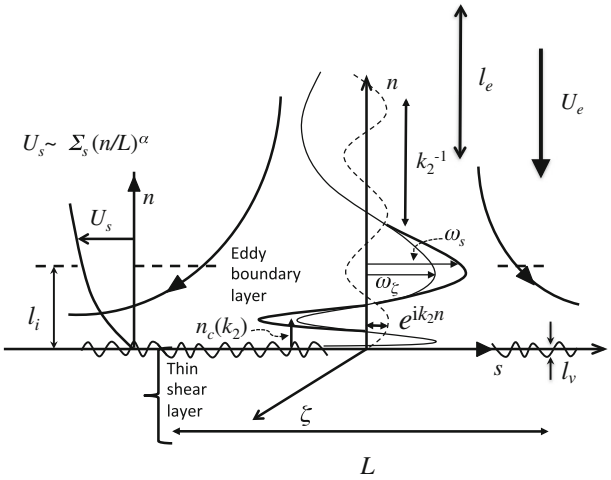

Fig. 9 Schematic diagram of a typical wave packet initially of wave-length ℓ_o with velocity u_e distorted by a larger eddy with velocity U_e and scale L impacting on the thin shear layer. The large eddy forms a boundary layer of thickness ℓ_i as it moves over the thin shear layer. Note how as the vorticity component ω_s is stretched and the normal length scale is reduced, the contribution to the transform of $\tilde{\omega}_s(k_2)$ becomes greatest in physical space where $k_2^{-1} \sim n_c$. This distortion determines the power law form of its velocity spectrum (integrated over space) $E(k) \propto k^{-2p}$ when $kL \gg 1$, where $2p$ depends on the form of the large eddy. Note that the energy of the small scale turbulence varies with distance n from the interface

cited by Hunt [20]. But the analysis demonstrated that only certain types of interaction lead to a quasi-equilibrium form of the average energy spectrum. This also leads to the conclusion that there must be a flux of energy into the thin layer at the interface. As the larger scale eddies separate from the interface, the smaller scale eddies are elongated and lead to local upscale transport. Although strong external eddies (or external forcing) with velocities greater than u could break through the layers (e.g. [15]), this is a rare event. Evidence of these processes was presented in IKH and Section 2.2. A local dynamical and statistical analysis is developed based on these mechanisms and these geometrical assumptions. The results are compared with the predictions of KO theory for second and some third moment statistics in the inertial range.

In Section 3.3 the order of magnitude of the fluctuating vorticity within the layers is estimated in terms of the external fluctuations of the impacting eddies as they are amplified by the shear in the layer, but damped by viscosity. The non-Gaussian characteristics [68] of the fluctuations and the marked differences between average and peak values are estimated by considering the sheltering mechanism which only allows larger external fluctuations to penetrate the layer [19, 69]. The smallest length scale of the typical microscale structures within the significant thin shear layers agrees with the usual KO estimate, defined in terms of the kinematic viscosity ν, and the average rate of dissipation for the whole flow ($\langle\epsilon\rangle$). But our analysis of the local mechanisms in these layers shows that the characteristic magnitudes of vorticity and velocity scales are much larger than the KO estimates, in agreement with the simulation results in IKH.

3.2 Inertial range interactions

3.2.1 Large eddy distortions near the thin shear layers

The analysis (following [21]) calculates how small scale eddy motions $\mathbf{u}(\mathbf{x}, t)$ with typical velocity u_e, and length scales ℓ_e are distorted and advected by quasi-steady larger motions $\mathbf{U}(\mathbf{x})$ of scale L where $\ell_e \ll L$, as they impact on and are blocked by the thin shear layers with thickness ℓ (see Figs. 8 and 9). Through local dynamics they maintain their sharply defined structure [15]. Note that L is less than the largest outer scale Λ associated with motions that advect the whole layer (see Fig. 7). The local analysis in $\mathcal{R}_o$ is in the frame of the moving layer using the local coordinate system $\mathbf{x}(s, n, \zeta)$ where the thin shear layer ($n < 0$) lies below the plane at $n = 0$. The rms value of $\mathbf{U}$ is U_e (averaged in a region outside the layer). The total velocity of the large scale and small scale motion in the frame relative to the mean interface (which undulates on a scale z_0 less than ℓ) is

$$\mathbf{u}^* = \mathbf{U} + \mathbf{u} = (U_s, U_n, U_\zeta) + (u_s, u_n, u_\zeta) \tag{1a}$$

(see Fig. 8). Note that the notation differs from Section 2 where fixed coordinates are used. The large scale flow field $\mathbf{U}(\mathbf{x})$, defined outside the layer (i.e. $n > 0$), is denoted for two- or three-dimensional motions by $\mathbf{U}^{(2)}(s, n)$ or $\mathbf{U}^{(3)}(s, n, \zeta)$. Because of the shear stresses, a turbulent boundary layer forms with thickness ℓ_i relative to the large eddies (as is observed in convective turbulence) as they impact on the interface [70]. If the small scale fluctuations have a small enough amplitude (i.e. $u_e < U_e$) then on the time scale of the distortion of the small eddies L/u_e, they do not affect the large scale blocking motions. The effect of the blocking and shearing on $\mathbf{u}$ is represented by

$$\mathbf{U} = \mathbf{U}^{(H)} + \Delta\mathbf{U}, \tag{1b}$$

where $\mathbf{U}^{(H)}$ is the large scale motion away from the thin layer and $\Delta\mathbf{U}$ is the perturbation. As with other blocked eddy motions [20], outside the surface boundary layer where $n \gg \ell_i$, the perturbations $\Delta\mathbf{U}$ are incompressible and approximately irrotational, and tend to zero away from the interface where $n \sim L$. They have to be matched to conditions near the interface. Thus, for $n > \ell_i$,

$$\nabla \cdot \Delta\mathbf{U} = 0, \quad \nabla \wedge \Delta\mathbf{U} = 0, \tag{1c}$$

but as $n/L \to 0$, where $\mathbf{U} \to 0$,

$$\Delta\mathbf{U} \cdot \mathbf{n} = -\mathbf{U}^{(H)} \cdot \mathbf{n} \quad \text{and} \quad \Delta\mathbf{U} \wedge \mathbf{n} \sim \mathbf{U}^{(H)} \wedge \mathbf{n}. \tag{1d}$$

Thus for a two-dimensional straining flow outside the boundary layer, since $L \gg \ell_i$,

$$\mathbf{U}^{(2)} \simeq (U_{sp} + \Sigma s, -\Sigma n, 0), \tag{2a}$$

where U_{sp} is the large scale velocity at a local stagnation point (SP) where $s = n = \zeta = 0$. Here Σ is the strain rate $\Sigma \sim U_e/L$. If $\mathbf{U}(\mathbf{x})$ is three-dimensional, ($n > \ell_i$)

$$\mathbf{U}^{(3)} = (U_{sp} + \Sigma_1 s, \Sigma_2 n, \Sigma_3 \zeta), \text{ where } \Sigma_1 + \Sigma_2 + \Sigma_3 = 0. \tag{2b}$$

In the special case of axisymmetric strain, ($n > \ell_i$)

$$\Sigma_1 = \Sigma_3 = -(1/2)\Sigma_2. \tag{2c}$$

In the scaling analysis Σ_2 is denoted by Σ. Depending on its sign, if $\Sigma \geq 0$ or < 0 the large scale eddy motion are like a stagnation or a separation point flow. Below $n = 0$, over the time scale larger than ℓ/u_e there is a persistent thin shear layer, with thickness ℓ. Fluctuations within the layer of scale ℓ_v cause fluctuations on edge of the layer, so that the interface near $n = 0$, has 'roughness' modulations also of scale ℓ_v, which are analysed in Section 3.3 (see [71]). Applying the boundary conditions (1d) to match Eq. 2a where $n \geq \ell_i$, an approximation for $\mathbf{U}^{(2)}$ is

$$\mathbf{U}^{(2)} = (\Sigma s G_1(n/L), -\Sigma n G_2(n/L), 0), \tag{3a}$$

where

$$G_1 = \frac{\mathrm{d}}{\mathrm{d}\hat{n}}(\hat{n}\ G_2) \text{ and } \hat{n} = n/L. \tag{3b}$$

Zilitinkevich et al. [70] showed that the profile of the tangential velocity component U_s, as each large eddy impacts on the interface, is logarithmic, i.e.

$$G_1 \ \propto \ \ln(n/z_0), \tag{3c}$$

where $z_0 \sim \ell_v$. But when $n/L \gtrsim 1/10$, the mean profile is affected by the external eddies and (as in the convective problem)

$$G_1 \ \sim \ (1 - \beta(n/\ell_i)^{-q}), \quad \text{where } 0 < q < 1. \tag{3d}$$

Since $\ell_i \propto L$, combining these formulae (as in boundary layer models), leads to the approximate expressions,

$$G_1 \simeq (n/L)^{\alpha} \text{ and } G_2 \simeq (n/L)^{\alpha}/(1+\alpha), \quad \text{where } 0 \leq \alpha \leq 1. \tag{3e}$$

Here $\alpha = 0$ is irrotational flow and $\alpha = 1$ corresponds to a stagnation layer with constant eddy viscosity. Typically $\alpha \sim 1/2$. The magnitude of these profile terms depend on the relative boundary layer thickness ℓ_i/L.

3.2.2 Small eddy distortions

Now consider a small scale eddy packet with a typical internal scale $k_o^{-1} \sim \ell_o$ and velocity $u_o \sim u_e$, initially located at n_o, being distorted as it moves in the large scale flow field with velocity U_o towards the plane $n = 0$. The overall size of the eddy packet is assumed to be comparable to L and large compared to ℓ_e, when the eddy's initial location is n_o. This process of distortion is similar to that experienced by eddies when a uniform flow $U_o = (-U_{n_o})$ impinges on a bluff body of scale L [21]. Since the normal velocity $(-U_n)$ decreases towards the surface as the travel time $\Delta\tau(n)$ increases, the scale of the fluctuations decrease normal to the plane. As the parallel components U_s, U_ζ increase, the scale in these directions increase and small elongated vortices form parallel to the interfaces [72]. The linear distortion of the fluctuating vorticity $\boldsymbol{\omega}$ of the eddy is determined by the large scale strain, if at each point $|\boldsymbol{\omega}| \leq |\boldsymbol{\Sigma}|$. But over the life of the eddy, because the non-linear effects are relatively weak for components with greater distortion [56], the conditions for the linear strain to dominate for the largest component of $\boldsymbol{\omega}$ is that $|\boldsymbol{\omega}| \leq \Sigma L/\ell_o \sim U_o/\ell_o$ which is satisfied since $u_e \ll U_o$. Far from the layer where $n \sim L \sim n_o$,

$$\omega_{oi}(x,t) = R\big\{\hat{\omega}_{oi} \exp\big(\mathrm{i}[\kappa_{1o}s + \kappa_{2o}(n - U_o t) + \kappa_{3o}\zeta(-\kappa_{2o}U_o t)]\big)\big\}. \tag{4a}$$

Near to the plane, the magnitude of the local vorticity ω_i in terms of ω_{oi} is determined by the distortion $\gamma_{ij}(\mathbf{x})$ which is determined by the stretching of vortex lines by the large scale flow, i.e.

$$\omega_i(x,t) = \gamma_{ij}(\mathbf{x})\omega_{oj} \exp\left(\mathrm{i}[-\kappa_{2o}U_o\Delta\tau(n) + \kappa_{1o}(-\Delta s)]\right), \tag{4b}$$

where the 'drift' time lag is $\Delta\tau(n) = (1/U_o)\int_n^{n_o}(U_{n_o}/U_n - 1)\mathrm{d}n$, and the displacement parallel to the interface is

$$\Delta s = \int_n^{n_o}(U_s/U_o)\mathrm{d}n, \tag{4c}$$

so that in the impinging region where $\Sigma < 0$ and $|s| \ll L$ for planar strain,

$$\gamma_{11} \simeq 1/\gamma_{22} \simeq U_{n_o}/U_n \sim (L/n)^{\sigma_{2D}}, \tag{5a}$$

where $\sigma_{2D} = 1 + \alpha$, and for axisymmetric strain,

$$\gamma_{11} \simeq \gamma_{33} \simeq 1/\sqrt{\gamma_{22}} \simeq (L/n)^{\sigma_{3D}}, \tag{5b}$$

where $\sigma_{3D} = (1+\alpha)/2$. Thus in general $1/2 < \sigma < 2$ as the shear and strain vary. (Note that although the straining by the large flow $\mathbf{U}$ is both rotational and irrotational, the latter determines the rapid growth of the distorted vorticity. But the former tends to isotropise the fluctuations [56, 73].)

3.2.3 Fourier transform and energy spectra

The conditional Fourier transforms (F.T.) of the vorticity fluctuations $\tilde{\boldsymbol{\omega}}$ are calculated for an ensemble of small scale eddies in a typical impaction region $\mathcal{R}_o$ outside a thin layer. Subsequently we consider the ensemble of all such regions. In previous studies of impinging turbulence (e.g. [21]), the wavenumber or frequency spectra were defined for homogeneous directions or steady conditions, not for coordinates with high non-uniformity, where the methodology was reviewed by Farge et al. [74]. The analysis (and flow visualization) shows that the F.T. and spectra for high wave numbers where $|\boldsymbol{\kappa}| \gg \kappa_o$, are the greatest for those wave numbers directed normal to the plane i.e. $k = |\kappa| \sim |\kappa_2|$. For each value of α depending on shear and strain, this is evaluated for the largest vorticity components, i.e. ω_1 in plane strain (or ω_1, ω_3 in axisymmetric strain). We consider for each type of strain / shear a conditional F.T. denoted by superscript (c) where $\widetilde{\omega_1}(\kappa_2)$ is the Fourier Transform of ω_1 in the normal direction (for a function defined in a domain of scale $L_S \sim L$) [21, 75]. Thus in the impinging region

$$\widetilde{\omega_2}(\kappa_2) \sim 1/2\pi \int_0^\infty \gamma_{11}\widetilde{\omega_{o1}} \exp\left(\mathrm{i}[-\kappa_o U_o \Delta\tau(n) + \kappa_o n + \kappa_2 n]\right)\mathrm{d}n \tag{6}$$

for a typical small eddy where $\kappa_{2o} \sim \kappa_{1o} \sim \kappa_o$, and $\kappa_o L \gg 1$. For the high wave numbers $\kappa_2 \gg \kappa_o$, there are rapid variations with n of $\exp(-\mathrm{i}\kappa_o U_o \Delta\tau(n))$ near the interface (see Fig. 9). Thence the main contribution at a given κ_2 comes from the

integral near $n = n_c(\kappa_2)$, where the local scale on which ω_c varies is comparable to ${\kappa_2}^{-1}$, which is the method of stationary phase. Thus n_c is determined by

$$\kappa_2 = \kappa_o - \kappa_o U_o \left(\frac{\mathrm{d}\Delta\tau}{\mathrm{d}n}\right)_{n=n_c} \text{ whence } \kappa_2 = \kappa_o(U_{n_o}/U_{n_c}) \sim \kappa_o(L/n_c). \tag{7a}$$

Thence for $\kappa_2/\kappa_o \gg 1$, i.e. $n_c(\kappa_2) \sim L(\kappa_o/\kappa_2)^{1/(1+\alpha)}$,

$$\widetilde{\omega_1}(\kappa_2) \sim \widetilde{\omega_{o1}}/(2\pi\kappa_o) \int_{-\infty}^{\infty} (L/n_c)^{(1+\alpha)} \exp\left[-\frac{\mathrm{i}}{2}\kappa_o U_o \left(\frac{\mathrm{d}^2\Delta\tau}{\mathrm{d}n^2}\right)_{n=n_c} n'^2\right] \mathrm{d}n', \tag{7b}$$

where

$$\left(\frac{\mathrm{d}^2\Delta\tau}{\mathrm{d}n^2}\right)_{n=n_c} = \frac{\mathrm{d}U_n/\mathrm{d}n}{U_n^2} \sim (L/n_c)^{(2+\alpha)} \sim (\kappa_2/\kappa_o)^{(2+\alpha)/(1+\alpha)}. \tag{7c}$$

Thence

$$|\widetilde{\omega_1}(\kappa_2)| \sim |\widetilde{\omega_{o1}}(\kappa_o)/2\pi|\, 2(L/\kappa_o)^{1/2}(\kappa_2/\kappa_o)^{p_\omega}, \tag{7d}$$

where for planar straining

$$p_\omega = 1 - \frac{2+\alpha}{2(1+\alpha)} = \frac{\alpha}{2(1+\alpha)}. \tag{7e}$$

Note that the exponent p_ω is determined both by the vortex straining and the wave length compression.

Note that a small proportion of the incident small scale eddies are not governed by this model where their length scales ℓ_e are very small compared to ℓ_o, with a velocity scale u_e, so that their vorticity ω_e can be greater than and not correlated with the large scale strain Σ, i.e. $\ell_e \leq u_e L_S/U_e$. Such eddies are not affected significantly by the large scale strain. But this contribution to the dynamics of the energy spectrum is small. However, eddies with initial vorticity ω_e comparable with or smaller than the large scale strain (Σ), are selectively organized and highly distorted, so that they continue receiving energy from the strain even when their vorticity exceeds Σ [56]. Note that the components of velocity that are reduced by the linear distortion begin to be amplified by the non-linearities and the smaller scale eddies become more isotropic.

Thus most of the small scale vorticity near the interface results from the distorted forms of intermediate scale eddies originally with scale $\ell_o \lesssim n_o$ as they are advected by the large scale motions. As shown above this leads to a self similar structure with a small scale 'power law form' of the amplitude of the Fourier Transform and spectrum, where the exponent p_ω only depends on the geometry of the distortion [57, 74].

Thus over the range of shear profiles i.e. $0 < \alpha < 1$, it follows from Eq. 7e that for plane straining

$$0 < 2p_\omega < \frac{1}{2}. \tag{8}$$

By the same analysis, the critical value of $n_c \sim \kappa_2^{-1}$ is the same for axisymmetric strain. But the vortex stretching is weaker, as $n/L \to 0$ and the change in γ_{11} leads to

$$2p_\omega = 1/(1+\alpha), \tag{9a}$$

so that

$$\frac{1}{2} < 2p_\omega < 1. \tag{9b}$$

For very high wave numbers Fourier Transforms of the velocity fluctuations $\tilde{\mathbf{u}}$ induced by the vortex stretching in the directions (s, ζ), parallel to the interface, are significant in all three velocity components (see below) so that outside the interface $(0 < n \lesssim L)$,

$$|\tilde{\mathbf{u}}| \sim |\tilde{\boldsymbol{\omega}}|/|\kappa_2|, \tag{10a}$$

where $\tilde{\mathbf{u}}$ and $\tilde{\boldsymbol{\omega}}$ are larger near $\kappa_2 \sim n^{-1}$. The conditional form of the velocity F.T. is simply related to the vorticity energy spectrum for strained components in Eq. 7d, so that for $\kappa_2 L \gg 1$,

$$|\widetilde{\mathbf{u}}|^2\,(\kappa_2) \sim \kappa_2^{-2}\,|\widetilde{\boldsymbol{\omega}}|^2 \tag{10b}$$

for $L^{-1} \ll \kappa_2 < \ell^{-1}$ in the domain $\mathcal{R}_o$. Thence from Eq. 7 for a wave packet with initial scale $\ell_o \sim k_o^{-1}$, when $k \gg \ell_o^{-1} > L^{-1}$ the energy is greater where the other wave numbers $|\kappa_1|, |\kappa_3|$ are of order k_o. Hence the three-dimensional F.T. is related to the one-dimensional F.T. by $|\tilde{u}_1|^2(k) \sim L_o^2 |\tilde{u}|(\kappa_2)$ where $|\kappa_2| \sim k$. The main contribution to the conditional energy spectrum for three-dimensional high wave numbers is therefore

$$E_X^{(c)}(k) \sim B_X^{(c)} k^{-2p} \tag{10c}$$

for an impinging wave packet with scale $\ell_o \sim k_o^{-1}$ and domain scale L, where $-2p = 2p_\omega - 2$. $B_X^{(c)}$ is determined by the spectrum of the wave packet and, via the exponent p, the form of straining by larger eddies. Thus

$$B_X^{(c)} = {E_0}^{(c)}(k_o) L^{2p}. \tag{10d}$$

Since $\ell_o \lesssim L$, the order of magnitude of ${E_0}^{(c)} \sim u_0^2 L$.

Depending on the form of the large scale shear, the exponent p changes; for plane straining,

$$2 \geq 2p \geq 3/2 \tag{11a}$$

and for axisymmetric straining

$$3/2 \geq 2p \geq 1. \tag{11b}$$

As small three-dimensional eddies on scale $\ell_e \ll L$ are advected into the stagnation regions their energy $\overline{u^2}$ is increased by a factor of approximately (n_o/n) [16].

Even though each Fourier component of the small scale normal velocity u_n is blocked by the thin shear layer, because the large scale straining keeps reducing the normal length scale of the distorted eddies and amplifying the vorticity, the result is that the mean square of u_n increases monotonically towards the interface (see [21], Figs. 10 and 11). Thence the rate of increase of small scale energy production in an eddy as it approaches the interface is of the order of $U_n \partial \overline{u^2}/\partial n \sim (u_o{}^3/L)(L/n)^{(1-\alpha)}$, which becomes very large near the interface. Also the smallest length scale (in the normal direction) of the most energetic component ω_e decreases in proportion to (n/n_o).

So far we have considered large scale motions impacting on the interface i.e. $U_n < 0$, which are regions of down-scale energy transfer. But as indicated in Fig. 8 the large scale eddy motions must also separate from the interface i.e. $U_n > 0$. In this part of the flow field the vorticity components that have been stretched parallel to the surfaces $(\omega_1(n), \omega_3(n))$ from a position n from the surface as they move away to a position n_s are then compressed by the convergence of the stream lines of the large eddies, i.e. $\omega_1(n)/\omega_1(n_s) \sim U_n(n)/U_n(n_s) \sim (n_s/n)^{\alpha}$, i.e. the reversal of the impacting process. To the first approximation (in u_e/U_o) these eddies are reversibly distorted as they are advected into adjacent separation zones, which is why these zones are regions of negative production of small scale energy and upscale energy transfer. This physical model broadly explains that the zones of local up and down scale energy transfer are adjacent to each other near the thin layers and also why they are approximately in balance as observed in data-analysis by Aoyama et al. [40]. The average value (in the zone $\mathcal{R}_o$) of $(\partial u_n/\partial n)^2$, is greater than u_e^2/ℓ_e^2 in the impinging eddies which have a singular distortion as $n \to 0$, and less in the convergent separating flow zones where eddy scales are less than k^{-1} [15]. Near

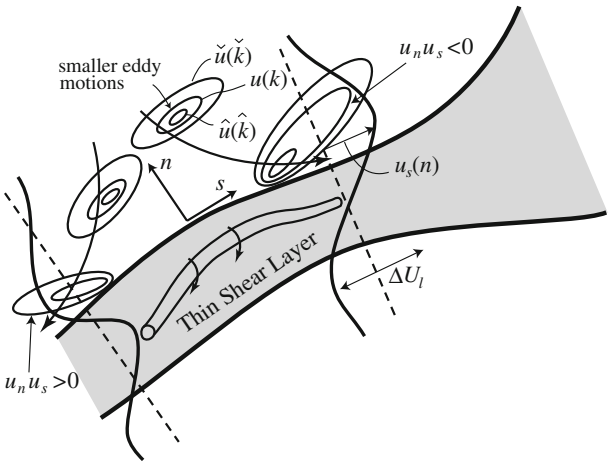

Fig. 10 Schematic diagram for the non-linear inhomogeneous (Obukhov-Townsend) model of how the distorted eddies (of scale $\breve{k}^{-1}$) larger than the scale k^{-1}, i.e. $\breve{k}^{-1} > k^{-1}$ located at $n \sim k^{-1}$ with velocity $\breve{u}(\breve{k})$ interact with smaller eddies of scale $\hat{k}^{-1} < k^{-1}$ with velocity $\breve{u}(\hat{k})$ centered at $\hat{k}^{-1}$. As a result of the correlation between the shear stress $u_n u_s$ and the local streamwise fluctuation, u_s, there is a local flux of energy F_ℓ directed to the interface of the thin layer leading to local equilibrium and persistence of the eddy structure

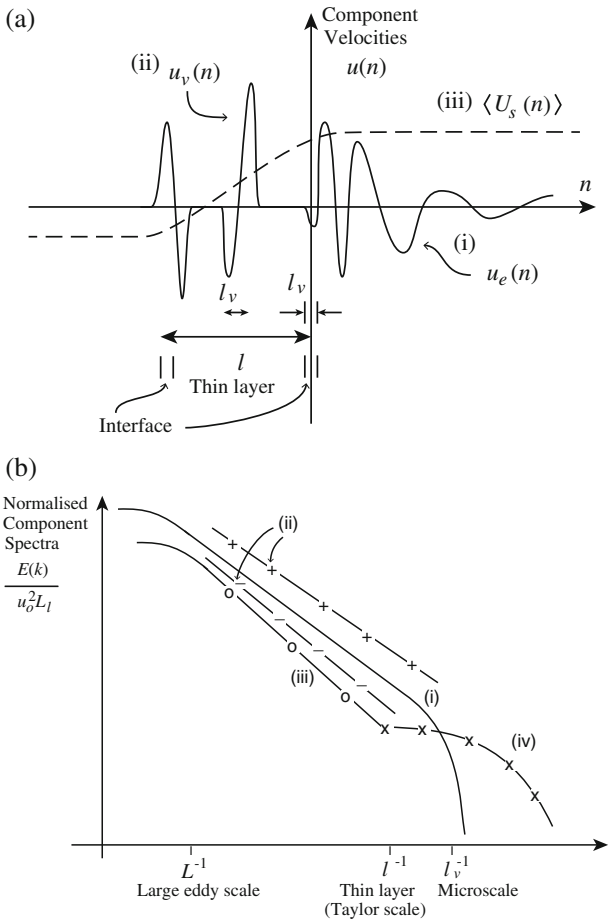

Fig. 11 Characteristic profiles and energy spectra of the components of the velocity field over the inertial and viscous range outside and inside the significant thin viscous layers. **a** (i) Typical velocity profile of a distorted small scale eddy $u_e(n)$ outside the thin shear layer where their energy contributes to the inertial range spectrum. (ii) Profile of characteristic microscale vortices within the thin shear layer $u_v(n)$. (iii) Coarse grained tangential velocity profile across the thin layer, $\langle U_s(n)\rangle$. [Note the magnitude of all these velocity components are of the same order, u_o. But, because of the different length scales and spatial distributions their spectra are different] **b** Energy spectra of the velocity (near the thin shear layers) (i) $E(k) \sim \langle\epsilon\rangle^{2/3}k^{-5/3}$ for $k \lesssim \ell_v^{-1}$, the local equilibrium spectrum (*solid line*) in the inertial range, with 'cut-off' at $k \sim \ell_v^{-1}$ resulting from the interface layer. (ii) $E^{(c)}(k)$ conditional spectra (+, −) of the distorted eddies that are not in equilibrium. (iii) $E_{v\ell}(k) \sim (u_o^2/L)k^{-2}$ for $k \lesssim \ell^{-1}$ spectrum in the inertial and viscous range associated with the vorticity of the thin shear layer (∘). (iv) $E_{v\ell}(k) \sim (\frac{u_o^2}{L}\ell\ell_v)\exp(-k\ell_v)$ for $k \gtrsim \ell_v^{-1}$, spectrum in the viscous range associated with the microscale vortices (×). Note that the component of the spectrum (i) dominates in the inertial range while component (iv) dominates in the viscous range $k > \ell_v^{-1}$ where $\ell_v \sim \ell/({R_\lambda}^{1/2}) \sim (\nu^3/\langle\epsilon\rangle)^{(1/4)}$

the upwind interfaces, where the large scale flow defined in fixed coordinates is directed into the shear layer, the impacting fluctuations are larger than at downwind interfaces. Hence the energy transfer into the thin shear layers is also greater near

the upwind interface, which leads to greater energy within the thin shear layer on the upwind side (as shown in IKH).

The correlation between the stretching of vortex lines and the strain within the stagnation/separation of zones adjacent to thin shear layers also determine the skewness S_K of the velocity derivatives. The finite and approximately constant value of S_K is one of the main characteristics of all homogeneous turbulent flows [35, 76]. In the former zones, where $\partial U_n/\partial n < 0$ (in notation of Fig. 9), $\langle(\partial u_n/\partial n)^2\rangle$ as the average value in the zone is amplified, it exceeds u_o^2/ℓ_o^2 [21] and in the latter $\partial U_n/\partial n > 0$, $\langle(\partial u_n/\partial n)^2\rangle$ is less than $\left(u_o^2/\ell_o^2\right)$. So that over a region including both kinds of zone, from the definition in Eq. 1a, $\langle(\partial u_n^*/\partial n)^3\rangle \sim \langle(\partial u_n/\partial n)^2(\partial U_n/\partial n)\rangle < 0$ (see Section 2.2.1 and Fig. 9a of IKH).

Therefore the skewness of the derivatives in the zone outside the thin shear layer

$$S_k = \langle\left(\partial u_n^*/\partial n\right)^3\rangle/\langle\left(\partial u_n^*/\partial n\right)^2\rangle^{3/2} \sim -1 \tag{12}$$

as the numerical and experimental data shows $S_k \cong -1$, with weak dependence on Reynolds number [77].

3.2.4 Non-linear energy transfer near the interface

The linear mechanism for the distortion of small scale eddies by larger impinging eddies reaches a maximum near the interface at $n = 0$. This distortion is reversed as the large eddy motions separate from the interface. However, during this reversible distortion process there is a non-linear interaction between the small eddies of decreasing scale near the interface, as noted in the computations of energy transfer between wave numbers given in Fig. 23 of IKH. As shown below this determines the net transfer of fluctuating energy into the thin viscous layers F_ℓ and also reduces the small scale anisotropy. The wind tunnel measurement by Britter et al. [65] of turbulence approaching a bluff body confirmed the theory of Hunt [21] that the energy containing motion of the incident turbulence become very anisotropic, but the degree of anisotropy of small scale velocity components of scale n at a distance n is within a factor of about 2. Experiments of vortices propelled onto rigid surfaces (e.g. [67]) demonstrate this distortion and quasi-isotropisation process.

The period over which this distortion of the small scales occurs is of the order of ℓ_e/u_e which is less than that of the large scale eddies ($\sim L/u_o$). Because the energy and length scales of the distorted eddies are distributed inhomogeneously near the interface, a modification is needed of the Obukhov [4] and Townsend [16] model for the spectrum in terms of non-linear energy transfer $T(k)$ from eddies of wave number $\check{k}$ less than k with characteristic velocity $\check{u}(k)$, to the smaller eddies, with wave number $\hat{k}$ greater than k with characteristic velocity $\hat{u}(k)$. In this locally inhomogeneous flows outside the thin layers, denoted by suffix X, these characteristic eddy velocities are defined by the square root of the energy spectra in Eq. 10c integrated over 0 to k, and from k to ∞, respectively. As the previous analysis has shown the distortion and therefore the non-linear interactions differ between the forms of the large impacting eddies. We denote the energy spectrum of different classes of distorted eddy as $E_X^{(c)}$. The distribution and magnitude of the quasi-independent eddy motions associated with scales k^{-1}, are approximately determined by their power law spectra when p is not an integer [57]. In the case of impinging eddies (like motion in spiral eddies) the transforms are dominated by

eddies $\hat{u}(k)$ at over a restricted range of space, in this case $n \sim 1/k$. The eddy concept here is similar to that used in the analysis of Section 3.3 of IKH.

The transfer of energy from larger to smaller scales and the form of the spectra are approximately determined by the weakly non-linear model based on the linear concept that the strain rate $(\partial \check{u}/\partial n)$ of larger scale eddies with scale $\check{k}$ amplifies the energy of the smaller scale fluctuation $\hat{u}$ with scales $\hat{k}$ less than k^{-1}. Following [4] and [16] the rate of energy transfer per unit mass to eddies with scale less than k^{-1} for this range of eddy motions outside the thin shear layers is denoted by $T_X^{(c)}(k)$

$$T_X^{(c)}(k) \sim \frac{\partial \check{u}}{\partial n} \cdot \hat{u}^2 \sim \left[\int_0^k \check{k}^2 E_X^{(c)}(\check{k})\, \mathrm{d}\check{k} \right]^{1/2} \cdot \int_k^\infty E_X^{(c)}(\hat{k})\, \mathrm{d}\hat{k}. \tag{13a}$$

This model is extended here, as a conditional model, for certain classes of large and small scale eddy motion in the highly inhomogeneous flow near an interface.

The average transfer over the ensemble of all the impact regions is denoted by $T_X(k)$. Note that in the RDT approximation (as bluff body experiments have demonstrated [65]) the length scale $\hat{k}^{-1}$ of the strained eddies can be of the same order as the length scale of the straining flow, in this case $\check{k}^{-1}$. The simulations by [38] showed that this is the optimum size relation of $\hat{u}$ and $\check{u}$ for eddy transfer. It is now assumed that (following [56], and Section 3.2.3) as the eddies become distorted non-linearly, the form of the non-linear energy spectrum $E_X^{(non-lin)}(k)$ is approximately unchanged, i.e.

$$E_X^{(non-lin)}(k) \sim E_X^{(lin)}(k), \tag{13b}$$

where $E_X^{(lin)}(k)$ is the energy spectrum given by the linear model.

Note that if $E_X^{(c)}(k) \propto k^{-2p}$ is substituted into Eq. 13, then the integral over $\check{k}$ converges if $2p < 3$ and the integral over $\hat{k}$ converges if $1 < 2p$. If these conditions are satisfied then the energy transfer $T_X^{(c)}(k)$ is dominated by the nonlinear interactions that are local in the wavenumber space. (Note that in the linear (RDT) model in Section 3.2.2, it is assumed that the distant (in the wavenumber space) interactions are dominant.) It is assumed in the present model that the approximations for the energy transfer $T_X^{(c)}(k)$ and the spectrum $E_X^{(c)}(k)$ based on the linear model may be approximately extrapolated to the nonlinear regime. In the present model it is assumed that since the turbulence is three-dimensional, its anisotropy does not significantly affect the form of the eddy transfer process.

These interactions between eddies on different scales determine the forms of the spectra near the interface. From Eq. 13 it follows that (only considering the physically significant cases where $3 > 2p > 1$)

$$T_X^{(c)}(k) \sim B_{X_T}^{(c)} \cdot k^{3/2(5/3-2p)}, \quad \text{where } B_{X_T}^{(c)} = \left(B_X^{(c)}\right)^{3/2} \tag{14a}$$

and $B_X^{(c)}$ is the dimensional variable in Eq. 10d depending on the larger scale straining eddies and the energy of the small scale eddies.

From the definition of $T_X^{(c)}(k)$, the rate of change of energy spectrum for unsteady turbulence is related to $E_X^{(c)}(k,t)$ (averaged over all the small eddies in one type of large eddy impact region)

$$\frac{\mathrm{d}}{\mathrm{d}t}\int_{k'}^{k''} E_X^{(c)}(k)\mathrm{d}k - \left(T_X^{(c)}(k'') - T_X^{(c)}(k')\right) = 0. \tag{14b}$$

Since Eq. 14 shows that, depending on whether the value of the exponent $2p$ is less or greater than 5/3, either the energy is building up ($\left(\frac{\mathrm{d}}{\mathrm{d}t}\right) E_X^{(c)}(k) > 0$) at high wave numbers in the straining region near the interface or is decreasing. For either of these types of eddy interaction where $2p \neq 5/3$ the local turbulent structure would be rapidly changing and would not persist. This would not be consistent with the numerical and experimental observation or the model concept that the turbulence is in a state of locally quasi-equilibrium, when averaged over all the large structures impinging/separating from the interfaces in the frame moving with the thin layer.

Thus for the dominant eddy structure, which determines the mean statistics, the transfer function $T_X(k)$ is constant for all wave numbers in the inertial range outside the thin layer, which is denoted by T_{Xeq}, i.e.

$$T_X^{(c)}(k) = T_X(k) \sim T_{Xeq} \text{ when } 0 < n \ll L. \tag{15a}$$

This is consistent with Eq. 13.

Therefore the value of p for the dominant range of eddy structures that produce small scale turbulence with the greatest persistence is

$$2p = 5/3 \tag{15b}$$

and from Eq. 15a, for the persistent structure over all impact regions, the coefficient in the spectrum is

$$B_{X_T} = T_{Xeq}, \tag{15c}$$

and from Eqs. 10c and 14a

$$E_X(k) \sim (T_{Xeq})^{2/3} k^{-5/3}. \tag{15d}$$

This implies from Eq. 11a that the inertial range spectrum in the exterior region is determined by plane structures and their interactions with the thin layers. Also these non-linear interactions of the distorted inhomogeneous small scale eddies near the interface tend to make these motions isotropic during the time scale of the large eddies because many of these interactions are on the same time scale (see Section 2).

The main contribution of the down-scale transfer to the small scale vorticity and velocity fluctuations of scale k^{-1}, occurs in a small region extending from the interface to a distance where $n \sim k^{-1}$. Consequently as energy is transferred to higher wave numbers, it is also effectively transferred to smaller scales near the interface. In the space with dimension of order L near the interface, the quasi-linear rapid straining of the smaller eddy motion by the large eddies impinging increases the energy of the eddy motions and affects the non-linear transfer from the large to smaller eddy scales. But there is neither an equivalent increase in viscous dissipation outside the thin layers (shown in IKH), nor energy advection of excess energy away from the external region outside the interface is the region of upscale transport (IGK).

Consequently there is a net transport of energy to the thin layers. By considering the mean turbulent energy equation per unit mass (e.g. [76]), in the moving frame

$$F_\ell = F_n(n=0) = -\left\langle u_n^* \left(\frac{u_i^{*2}}{2} + p^* \right) \right\rangle, \tag{16a}$$

where $u_i^{*2}/2$ is the kinetic energy of the fluctuation relative to the interface (i.e. the large eddies and the small eddy motion) and is the fluctuating pressure (normalized on density).

Studies of two-point cross correlation in sheared and shear-free turbulent boundary layers at very high Reynolds number [20, 78] have shown that the blocking mechanism at the surface determines that the length scale of the normal components of eddy motion is of order n, the distance from the resistive interface at $n = 0$; i.e. eddies centered at higher n, with length scale n are inducing fluctuations at the interface [16].

Thus the flux of energy to the interface F_n has contributions from eddies of all scales up to order L. The dominant eddy structure producing this flux is the product $u_n u_s u_s$ of the local Reynolds shear stress $u_n u_s$ and the fluctuation u_s is the direction of the impinging eddies at the interface (Figs. 9 and 10). Both these terms are finite as $n \to 0$ at the interface and are continuous and u_s are continuous since they match the fluctuation within the thin layer (see Section 3.3). Note that F_ℓ depends on the mean value of the product.

This correlation can be estimated and related to the spectrum by considering how locally $u_n u_s$ and u_s vary near the interface. The large scale impinging flow field $\mathbf{u}$ leads to a positive shear flow near the surface where $s > 0$ and $\partial u_s/\partial n > 0$ (Fig. 9). This distorts the small-scale eddy motion, which induces a positive Reynolds stress (i.e. $u_n u_s < 0$), and thence the amplification of both ${u_s}^2$ and the shear $\mathrm{d}\check{u}_s/\mathrm{d}n$ of eddies larger than n. Note that where $s < 0$, $u_n u_s$ changes sign.

The distortion of the eddy scale motions, $\mathbf{u}$, in the shear flow near the interface (defined in Section 3.2.1) affects the non-linear transfer of energy from eddies of scale $\check{k}^{-1}$ to smaller eddies of scale $\hat{k}^{-1}$. This determines the magnitude of F_ℓ and its connection with the energy spectra.

The RDT model for the Reynolds stress co-spectrum $E_{sn}(k)$ in terms of $E(k)$ for homogeneous turbulence in a uniform large scale shear $\mathrm{d}u_s/\mathrm{d}n$, shows that in the inertial range [79],

$$E_{sn}(k) \sim -E(k) \frac{\mathrm{d}U_s}{\mathrm{d}n} \hat{\tau}(k). \tag{16b}$$

Here $\hat{\tau}(k)$ is the short relaxation time for eddies of scale k^{-1}, which is estimated from the physical arguments of KO theory, i.e.

$$\hat{\tau}(k) \sim \left[E(k) k^3 \right]^{-1/2}.$$

Thence the co-spectrum is a small perturbation from the KO isotropic homogeneous turbulence. This model leads to

$$E_{sn}(k) \sim -\langle \epsilon \rangle^{1/3} \frac{\mathrm{d}U_s}{\mathrm{d}n} k^{-7/3} \tag{16c}$$

(Wyngaard [42]).

This quasi-homogeneous result can be applied where $\mathrm{d}u_s/\mathrm{d}n$ is a variable quantity. Then the rms of the co-spectrum $E'_{sn}(k)$ of the Reynolds stress of the small scale

eddies $\hat{u}(\hat{k})$ is proportional to the rms gradient of the larger scale eddies $\check{u}(\check{k})$ (as previously estimated in Eq. 13a), where

$$\frac{\mathrm{d}\check{u}}{\mathrm{d}n}(k) \sim \left[\int_0^k \check{k}^2 E_X(\check{k})\mathrm{d}\check{k}\right]^{1/2}. \tag{16d}$$

Thus from Eq. 16b

$$E'_{sn}(k) \sim E_X(k)\left[E_X(k)k^3\right]^{-1/2}\left[\int_0^k \check{k}^2 E_X(\check{k})\mathrm{d}\check{k}\right]^{1/2} \sim E_X(k). \tag{16e}$$

By considering its contribution to the energy flux F_ℓ from all eddy scales, and because of the correlation (already explained) between $u_n u_s$ and u_s in the shearing region near the interface, it follows that

$$F_\ell \sim -\langle u_n u_s \cdot u_s\rangle \sim \langle (u_n u_s)^2\rangle^{1/2} \cdot \langle u_s^2\rangle^{1/2} \sim \int_{L^{-1}}^{\infty} E'_{sn}(\hat{k})\mathrm{d}\hat{k} \cdot \left(T_{Xeq} \cdot L\right)^{1/3}, \tag{16f}$$

where from Eq. 15d $\langle u_s^2\rangle^{3/2} \sim [\int_{L^{-1}}^{\infty} E(\hat{k})\mathrm{d}\hat{k}]^{3/2} \sim T_{Xeq} \cdot L$. Substituting Eq. 16f into Eq. 15d shows that the quasi-equilibrium energy spectrum (15d) is determined by the energy flux into the thin layers and not by local dissipation in $\mathcal{R}_o$ outside the layers. Thence

$$F_\ell \sim T_{Xeq} \cdot L. \tag{16g}$$

By considering the balance of energy across the thin layers, which are in approximate equilibrium, it follows that the average rate of dissipation within the thin layer per unit area, ϵ_ℓ is related to F_ℓ by $F_\ell \sim \epsilon_\ell \ell$. So that from Eqs. 15c and 16g T_{Xeq} is equivalent to the spectrum coefficient B_{X_T} and to the dissipation rate over the whole flow field $\langle\epsilon\rangle$, i.e.

$$T_{Xeq} \sim B_{X_T} \sim \epsilon_\ell \ell / L \sim \langle\epsilon\rangle. \tag{17}$$

Note that (as in the simulated turbulence, see Table 2 of IKH) the mean dissipation in the thin layer ϵ_ℓ is therefore significantly greater (by $O(Re^{1/2})$) than in the quasi-homogeneous region. Table 2 of IKH also shows that $T_{Xeq}/\langle\epsilon\rangle$ is greater on the side of the significant thin shear layer where the mean velocity points into the layer (i.e. upwind side) and less on the side it points outwards. But on both sides $T_{Xeq}/\langle\epsilon\rangle$ is much less than inside the layer. Thus B_T is the average value of energy transfer over all the eddy structures, so that Eqs. 16 and 10b lead to the average magnitude and form of the inertial range spectrum outside the thin layer $E(k)$. It follows that the magnitude of the inertial range spectrum associated with regions of scale L around the significant shear layers can be expressed in terms of the relevant physical variable T_{Xeq}, i.e.

$$E_X(k) \sim (T_{Xeq})^{2/3} k^{-5/3}. \tag{18a}$$

But from Eq. 16 this is equivalent to the model of KO in which the spectrum is expressed in terms of the average rate of dissipation $\langle\epsilon\rangle$, i.e.

$$E_X(k) \sim \langle\epsilon\rangle^{2/3} k^{-5/3}. \tag{18b}$$

Thus the model proposed here shows how the linear distortion of the local turbulent eddy structures, together with their weakly non-linear interactions and selection mechanism close to the interface (as seen in Fig. 23 and in Table 2 of IKH), determines the quasi-equilibrium local form of the inertial range second order spectrum outside the thin layer. Table 2 of IKH also shows that there is significant eddy transfer to small scales within the thin layer. Satisfying these results also agree with Eq. 18b for the inertial range. But note that the magnitude of high order moments are likely to differ more from the homogeneous KO model.

Note also that the model does not assume that the velocity or vorticity field near the interface are approximately isotropic. Measurements show that the spectrum (18) is valid over wave number where the fluctuations are not isotropic (to within a factor of 2 or 3) [43].

3.3 Dynamics of thin shear layers and viscous microscale eddies

3.3.1 Overall structure of the layers

We now consider an idealized model for the main features of the significant thin layers of thickness ℓ. It is observed that their curvature is small compared to $1/\ell$, and that they extend over distances large compared to ℓ, typically of order L_S, i.e. comparable with the distance between neighbouring layers (see Fig. 7). The layers are moving with the large scale flow $\langle \mathbf{U} \rangle$ (defined over L_S) and there is in general a mean velocity jump $\Delta \mathbf{U}_\ell$ (in the s direction—as in Fig. 9) across these layers, where $|\Delta \mathbf{U}_\ell| = \Delta U_\ell$ is of the order of the rms velocity u_o and $\Delta \mathbf{U}_\ell$ changes slowly with s (over distances of order L).

The thickness of the layer is determined partly by impact and shearing between large scale impinging eddies with velocity $U \sim u_o$ and scale L, which leads to a inertial-viscous shear layer e.g. [80] with thickness $\ell \sim L Re^{-1/2}$; such as the viscous shear layer around a high Reynolds number vortical eddy. Note that the rate of dissipation in such layers associated with the mean velocity is $\bar{\epsilon}_\ell \sim \nu \cdot {u_o}^2/\ell^2 \sim u_o^3/L \sim \langle \epsilon \rangle$. Thus $\bar{\epsilon}_\ell$ is of the same order as that of the mean dissipation in the turbulence outside the thin layers, i.e. $\bar{\epsilon}_\ell \sim \langle \epsilon \rangle$. This is much less than the high dissipation rate generated by the flux of the energy of the external eddies (ϵ_ℓ), which is considered below.

Note that the diffusion outwards of the high gradient of mean velocity within the thin layer is inhibited by the counter gradient effects of straining by the large external eddies-provided they are not so strong that they deform or destroy the interface [8, 15, 81]. Because the external straining is asymmetric, being greater on the upwind side, the external flow is also asymmetric. The interface between the external and internal flow structure has a finite thickness ℓ_i, which is observed to be significantly less than ℓ [31, 71], and is determined by the internal fluctuations, which are considered below.

3.3.2 Fluctuations and structures within the thin layers

In high Reynolds numbers turbulence, when external eddies with scale ℓ_e moving with a velocity u_e in a larger scale flow relative to the large scale velocity U approach a thin shear layer with thickness ℓ significantly less than ℓ_e, they may or may not induce significant fluctuations within the layer. If the eddy velocity u_e (in the

direction parallel to the layer) is approximately equal to U (the typical difference being of order u_e), the large scale fluctuations within the layer are much less than u_e—the sheltering effect [19, 69]. However, fluctuations on the scale of ℓ develop on the interface, which are then amplified by the mean shear in the layer (ΔU_ℓ) and in turn induce fluctuations across the whole layer [82]—as has been observed and simulated in boundary layers.

Linear analysis and computations of the distortion of the vorticity of non-normal fluctuations shows they grow as a result of the strain $\Sigma \sim \Delta U_\ell/\ell$, the compressed and extended length scales ℓ_c and L_e decrease and increase respectively (e.g. [73, 83]) until asymptotically the smallest scales reach the limiting viscous scale ℓ_v where viscous diffusion of vorticity balances the strain rate, where

$$\ell_v \approx \left(\frac{\nu}{\Sigma}\right)^{1/2}, \Sigma = \Delta U_\ell/\ell \sim (u_o/L)Re^{1/2} \sim (\langle\epsilon\rangle/\nu)^{1/2}. \tag{19a}$$

Thence in terms of $\langle\epsilon\rangle, \nu$;

$$\ell_v \sim (\nu^3/\langle\epsilon\rangle)^{1/4} \sim L \cdot Re^{-3/4} \sim L \cdot {R_\lambda}^{-3/2}. \tag{19b}$$

This estimate is for straining by the shear flow leading to vorticity components ω_s, ω_n in the s, n plane. The length of the vortical structure in the ζ direction, normal to the directions is not significantly changed by this mechanism. Because the vortices are flattened into strips by the straining, they then tend to 'roll-up' non-linearly and rapidly into vortices with radius ℓ_v (e.g. [56]). Significant vorticity fluctuations are also caused by the upward deflection and subsequent 'horse-shoe' distortion of the vortex lines of the mean shear [84]. The velocity induced by the horse-shoe structure locally amplifies the vorticity ω_ζ, up to the visco-inertial limit. This is why, as seen in the simulations (Fig. 3 of IKH), the amplified micro scale vortices in the thin layers lie in all directions.

The magnitude of the vorticity fluctuations is estimated based on stretching of the vortex lines with length L_e up to the visco-inertial limit and their initial vorticity $\omega_{\ell o}$ (produced by external fluctuations), which is of order of the mean vorticity of the layer, i.e. $\omega_{\ell o} \sim \Delta U/\ell \sim \omega_o Re^{1/2}$. This is much larger than $\omega_o \sim u_o/L$, the vorticity of the large scale eddies. The typical initial scales of the fluctuations are comparable with the layer thickness, ℓ since much larger scale internal fluctuations are not amplified in the shear layer. The planar distortion leads to $L_e \sim \ell \exp(\Sigma t) \sim \ell \cdot \ell/\ell_c$ for $\ell_c > \ell_v$.

Thence, the greatest lengths L_v of the micro vortices are of order $\ell \cdot \ell/\ell_v$, i.e.

$$L_v \sim \ell \cdot Re^{1/4} \sim L \cdot Re^{-1/4}. \tag{20a}$$

Therefore the microscale vortices are shorter than the external scale of large eddies L_S, but greater than the layer thickness by $O(R_\lambda^{1/2})$, which correspond to a factor of about 10 for the simulations (IKH) and experiments (Section 2; [51]).

For such isolated vortices $|\boldsymbol{\omega}| = \omega_v$ is proportional to the length of the fluid volume of the structure in the direction of $\boldsymbol{\omega}$ (e.g. [76]), i.e.

$$\omega_v \sim \omega_\ell(\ell/\ell_v) \sim \omega_\ell {R_\lambda}^{1/2} \sim \omega_o {R_\lambda}^{3/2}. \tag{20b}$$

Note that the magnitude of the vorticity of certain fluctuations (ω_v) can exceed that of the mean vorticity in the layer ($\omega_\ell \sim u_o/\ell$), because non-linear terms in the equation may not limit the growth of ω_v [56].

Thence from Eq. 20b the peak vorticity ω_v is greater by a factor ${R_\lambda}^{1/2}$ than the mean vorticity of the layer ω_ℓ, which is of the order of the rms vorticity of the whole domain $\omega_{\rm rms} = (2\Omega/3)^{1/2}$ (Table 1). ω_v is much greater than the integral scale vorticity, ω_o by $O({R_\lambda}^{3/2})$, i.e.

$$\omega_v \sim \omega_o Re^{3/4} \sim \omega_\ell Re^{1/4} \sim \omega_{\rm kol} Re^{1/4}. \tag{20c}$$

The fluctuating vorticity component ω_ζ parallel to the mean vorticity in the shear layer is of the same order as Eq. 20c for positive values (i.e. with the same sign as the local mean vorticity). But the length scale of the fluctuations in this directions are of the order of the "horseshoe" type of eddies which are of the order of the thickness of the layer, i.e. ℓ. These structures do not appear to be associated with elongated vortices in the flow direction. (See Fig. 3 of IKH).

The rms value of the microscale vorticity fluctuation averaged across the layer, $\omega_{\rm rms}^{\rm (Inside)}$, is of the order of $\omega_v/\tilde{\delta}_v^2$, where $\tilde{\delta}_v$ is the normalised distance between vortices, i.e. $\tilde{\delta}_v = (\delta^\pm/\ell_v)$ ($\delta^\pm$ is defined in IKH as the distance between the nearest-neighbor positive/negative ω_y peaks that satisfy a certain threshold $|\omega_y| > \gamma\omega_{\rm rms}^{\rm (Inside)}$). By contrast the KO microscale vorticity in the quasi-homogeneous regions outside the layer is determined by weak fluctuations distorted by large scale straining until limited by viscosity, so that $\omega_\ell \sim \omega_{\rm kol} \sim (\langle\epsilon\rangle/\nu)^{1/2}$ (see [29]).

The corresponding peak velocity difference u_v is of the order of the velocity jump across the thin layer or the rms velocity of the energy containing eddies. It is much greater than the homogeneous estimate $u_{\rm kol}$ for microscale vortices by $O({R_\lambda}^{1/2})$, i.e.

$$u_v \sim \omega_v \ell_v \sim u_o \sim u_{\rm kol} {R_\lambda}^{1/2}, \tag{20d}$$

where $u_{\rm kol} \sim (\langle\epsilon\rangle\,\nu)^{1/4}$. The average (i.e. local, rms) value of the smallest scale vorticity fluctuations in the layer is of the same order as ω_v since the spacing is of order ℓ_v.

The intense vortices in these layers dissipate energy locally at a rate

$$\epsilon_v \sim \nu(u_v/\ell_v)^2 \sim (u_o^3/L)R_\lambda, \tag{21a}$$

which is a factor R_λ greater than the average over the whole flow. This is related to the average dissipation across the layer ϵ_ℓ, in terms of the distance between the vortices, i.e.

$$\epsilon_\ell \sim \epsilon_v/(\tilde{\delta}_v^2/4) \sim \epsilon_v \tag{21b}$$

since $\tilde{\delta}_v \sim 2$ for typical vortices (see Section 3.2 of IKH).

These estimates can be compared with the simulations in IKH, summarised in Table 2, and also with the experimental results in Section 2. (Note that the order of magnitude theoretical estimates do not agree closely with all the detailed data, but that they are consistent with the overall structure of the turbulent flow.) The thickness ℓ of the significant thin layers where the rms vorticity $\omega_{\rm rms}^{\rm (Inside)}$ is 3.3 times greater than the rms vorticity $\omega_{\rm rms}$ for the whole flow is about 4λ, where λ is the Taylor microscale given in Table 1 of IKH. Within the thin layers, the thicknesses of the microscale vortices ℓ_v are computed to be about 10η, where $\eta = (\nu^3/\langle\epsilon\rangle)^{1/4}$. The strengths of the peak vortices ω_v, defined in Fig. 18 of IKH as $\gamma\omega_{\rm Inside}$, vary over a factor of 2. But there are some vortices with much greater magnitude.

Table 2 Characteristics (measured by IKH in the DNS of homogeneous turbulence at $R_\lambda = 1131$) of a strong thin shear layer and strong microscale vortices within the thin layer. For comparison with coherent structure model in Section 3.3.2, the mean vorticity across the layer $\omega_\ell \sim |\langle \boldsymbol{\omega} \rangle_{\text{Inside}}|$, fluctuations of vorticity $\omega_{\text{rms}}^{(\text{Inside})} \sim 3.3\omega_{\text{rms}}$. Note that the Kolomogorov microscale variables are $\omega_{\text{kol}} \equiv (\langle\epsilon\rangle/\nu)^{1/2} \sim 1.73\omega_{\text{rms}}$ and $u_{\text{kol}} \equiv (\langle\epsilon\rangle\nu)^{1/4} \sim 0.0585u_o$

ℓ_v :	$\sim 10\eta$,	ℓ :	$\sim 4\lambda$,	L_v :	$\sim 3\lambda \sim 0.1L$
ω_v :	$5.6\omega_{\text{rms}} - 35\omega_{\text{rms}}$,	ω_ℓ :	$0.78\omega_{\text{rms}}$,	$\omega_o(\sim u_o/L)$:	$0.014\omega_{\text{rms}}$,
u_v :	$\lesssim 3.4u_o$,	ϵ_v :	$\lesssim 85\langle\epsilon\rangle$,	ϵ_ℓ :	$\sim 10\langle\epsilon\rangle$

The thickness estimate broadly confirms Eq. 19b, and supports the concept that ℓ_v is determined by a quasi-linear mechanism, driven by random forcing by the exterior eddies over a wide range of amplitude. The model predicts (as explained below Eq. 20d) that the ratio of $\omega_{\text{rms}}^{(\text{Inside})}$ to ω_v depends on the normalised spacing $\tilde{\delta}_v$ which is not very sensitive to γ (Fig. 18 of IKH). Typically $\delta_v \sim 2\ell_v$. This implies that

$$\omega_{\text{rms}}^{(\text{Inside})} \sim \omega_v/\tilde{\delta}_v^2 \sim \omega_{\text{rms}} R_\lambda{}^{1/2}/\tilde{\delta}_v^2.$$

Thus if $R_\lambda \sim 10^3$ and $\tilde{\delta}_v \sim 1$, the model implies that $\omega_{\text{rms}}^{(\text{Inside})}/\omega_{\text{rms}}$ is about 30. Since the computations show that this ratio is about 3, it indicates that $\tilde{\delta}_v$ is about 3 for typical vortices.

The peak velocities in the vortices, denoted $\delta w/u_o$ in Fig. 16a of IKH, have a wide range of amplitude, because of the random external forcing. By integrating the probability density function in Fig. 13a from $\delta w/u_o$ equal to 0.3 to 3, it follows that the probability of a microscale vortex in a 'significant' thin shear layer having a magnitude of order u_o is about 0.3. This is broadly a confirmation of the prediction (20d).

3.3.3 Spectra and moments associated with significant thin layers

The velocity energy spectrum $E(k)$ in the high wave number range is determined by the inertial range eddies and the fluctuations generated by the intense vortices within the thin layer. But the contributions of these fluctuations are very small outside the thin layer because of the sheltering by the layer's vorticity. The velocity fluctuations in the normal direction induced by the vortices lead to elongated shearing motions or 'streaks' within the thin layer on the scale L_v; but as linear theory and DNS simulations of eddy structure in shear layers (reviewed by Hunt and Carruthers [73]). Lee et al. [83] show that for low wave numbers between the large scale $1/L_v$ and the small viscous scale of order $1/\ell_v$, the spectra are self-similar and typically proportional to k^{-q} where $q = 1$ or 2, depending on the initial form of the disturbances. (These were analysed for neutral and stratified flows by [85]). She and Jackson [86] introduced a model based on the spectral analysis of measurements that $q \sim 1$, for the terms that is a correction to the $-5/3$ and concluded that there might be a double structure of internal vortices and coherent structures. $q = 1$ is the low wave number exponent in many confined turbulent shear flows exhibiting a 'streaky' structure (e.g. [87, 88]).

There are also significant fluctuations, $\Delta u'$, in the jump velocity across the thin layer, with magnitude of order u_o. Consequently there are fluctuations of this order in the external region over the scale L.

Let $E_{v\ell}^{(c)}(k)$ and $E_X^{(c)}(k)$ be the conditional energy spectra over the 'local' space external and within the thin layer (i.e. with volume L^3), associated with the impinging

eddies and with the highly anisotropic internal layer fluctuations, respectively. Since the small scale motions in these local spaces are approximately independent of each other, the spectra for the significant layers (denoted by { }) over the whole domain are the average of the conditional spectra over all thin layers, i.e.

$$\{E(k)\} \sim E_X(k) + E_{v\ell}(k). \tag{22a}$$

There is a cut-off of E_X where k^{-1} is smaller than ℓ_{vi}, the thickness of the interface between the thin layer and the external flow. The spectrum for the fluctuations in the thin layer $E_{v\ell}$ extends to the smallest viscous scales of order ℓ_v. Since $\ell_{vi} \sim \ell_v$, this means that both spectra cover the viscous range of wavenumbers, but are not dependent on flow in the same regions of space (see Fig. 11).

An approximate model for $E_X(k)$ for the impacting motions of the external eddies is

$$E_X(k) \sim \langle\epsilon\rangle^{2/3} k^{-5/3} \exp[-C_X(k\ell_{vi})^{m_X}]. \tag{22b}$$

where C_X and m_X are non-dimensional positive constants, and the exponential decay term for $k > \ell_v^{-1}$ and the parameter m_X depend on how the external fluctuations at the edge of the thin layer adjust to the fluctuations within the layer, which could not be resolved in the simulations in IKH.

Another model is appropriate for $E_{v\ell}(k)$, to account for the visco-inertial eddy motions in the layers plus the contribution of the random jump velocities (ΔU_ℓ) across the shear layers and the internal velocity profile, i.e.,

$$E_{v\ell}(k) \sim (u_o)^2 L\left[(\ell/L)C_I H(k\ell - 1)/(kL)^q + C_s(kL)^{-2}\right] \exp[-C_v(k\ell_{vi})^{m_v}], \tag{22c}$$

where $H(\,)$ is the step function and C_v, m_v are non-dimensional positive constants which need not be specified for the following discussion. Note that the total energy of the internal fluctuations is confined within the layers. Hence the geometrical factor (ℓ/L) is introduced to model the spectra over the space of order L. C_I, the coefficient for internal fluctuations, which include peak values of order u_o, is at most of order 1. It is multiplied by a step function $H(\,)$, since its magnitude is reduced for $k < \ell^{-1}$ and since the internal fluctuations do not extend outside the layer as a result of shielding by the vorticity at the edges of the layers (e.g. [69]). The coefficient C_s for the spectra of fluctuations across the layer (which contribute to the spectra for wavenumbers over the range L^{-1} to ℓ^{-1}) is of order 1—as with all fluctuating vortex sheets.

Note that the velocity fluctuations associated with the fluctuating net shear across the layer induce a k^{-2} spectrum (as usual for step functions) in the external inertial range flow region, where $k\ell_v \ll 1$. For $k \gg 1/\ell_v$ there is a viscous scale cut off. Thus the two contributions in the inertial wave-number range (outside the thin layers), where $L^{-1} < k < \ell^{-1}$, which come from the impinging turbulence and the shear layer fluctuations, i.e. from Eq. 22

$$E_X(k) \sim (u_o)^2 L(kL)^{-5/3} \quad \text{and} \quad E_{v\ell}(k) \sim (u_o)^2 L(kL)^{-2}. \tag{23}$$

Note that the $-5/3$ inertial range is valid only when $L/\ell_v > (kL) \gg 1$. From Eq. 22 it follows that the ratio of E_X to $E_{v\ell}$ varies over this range. The criterion for

the inertial eddy spectrum to dominate over the second order shear layer induced spectrum over this whole wave number range is that $Re^{1/4} \gg 1$. For the simulations used here $Re^{1/4} \sim 10$, so the criterion is well satisfied. (This is the criterion that the smallest scale motions evaluated on the KO model are much larger than the largest scale strains [57].) The combined spectra from Eq. 22 suggest that the 'compensated' form for $E(k)$, (i.e. $k^{5/3}E(k)$), can increase slightly above the inertial range spectrum (22b) for a limited range of wave numbers near $k \sim \ell_v^{-1}$ if $\ell_{vi} < \ell_v$ (IKH, IGK).

Away from the significant thin layers, the quasi-homogeneous eddy motions have weaker microscale vortices vortices of magnitude $\omega_{\rm kol} \sim u_o/\lambda \sim \omega_\ell$ with the typical velocity fluctuations of magnitude $u_{\rm kol} \sim u_o/{R_\lambda}^{1/2}$, but their spectra $E_{qh}(k)$ have the same form as those associated with the thin layer (22b). This is because of the larger number of weaker (rather than stronger) structures per unit volume.

Higher order moments can indicate better than second order spectra the intermittency of the fluctuations in the thin layers (see Section 3.1 of IKH and Section 3.2.3). The simulations show that within the thin layers of thickness ℓ the vortices are close packed, with a typical spacing of order ℓ_v. It implies that the flatness factor of vorticity within the layer is determined more by their strength than by their spacing. From the exponential pdf of the velocity jumps δw in Fig 16a of IKH, since their thickness does not vary significantly and since the peak vortices in the specific layer have components predominantly parallel to y, it follows that the pdf of vorticity is also exponential, and therefore $\mathcal{F}\left[\omega_y\right]_{\rm Inside} \approx \mathcal{F}\left[\partial w/\partial x\right]_{\rm Inside}$. (Here local flatness factor of ϕ in a specific region $\mathcal{D}$ is defined by

$$\mathcal{F}[\phi]_{\mathcal{D}} \equiv \frac{\left\langle(\phi - \langle\phi\rangle_{\mathcal{D}})^4\right\rangle_{\mathcal{D}}}{\left[\left\langle(\phi - \langle\phi\rangle_{\mathcal{D}})^2\right\rangle_{\mathcal{D}}\right]^2},$$

where $\langle\phi\rangle_{\mathcal{D}}$ is the average of ϕ over the region $\mathcal{D}$. "*Inside*" denotes the region inside the specific layer (see IKH).) The simulations show that $\mathcal{F}\left[\partial w/\partial x\right]_{\rm Inside} \approx 6.0$ is much less than the flatness factor of $\partial w/\partial x$ over the whole domain $\mathcal{E}$, i.e. $\mathcal{F}[\partial w/\partial x]_{\mathcal{E}} \approx 15.6$. As shown in Fig. 14 of IKH, vortices in the thin layers have much larger gradients than in the distorted eddies outside the thin layers. Also, the spacing of the layers is of order L. If we assume that $\partial w/\partial x$ is negligibly small outside the layers, then $\mathcal{F}[\partial w/\partial x]_{\mathcal{E}}$ is estimated (using $L/\ell \approx 10$ from Table 1 of IKH) as $\mathcal{F}[\partial w/\partial x]_{\rm Inside} \times (L/\ell) \approx 60$, which is not far from the DNS value.

We conclude that the quasi-deterministic model for the random distribution of the strained microscale vortices in the viscous layers broadly agrees with the simulations. It also helps explain the limitations of the physical interpretations of the KO model that assumes a homogeneous distribution of microscale eddies. However, the KO prediction for the smallest statistical length scale ℓ_v in relation to the average dissipation rate $\langle\epsilon\rangle$ and ν, i.e. $\ell_v \sim \left(\nu^3/\langle\epsilon\rangle\right)^{1/4}$ does indeed agree with the observed average thickness of the microscale vortices in the significant thin layers (Table 2 and the experiments in Section 2).

3.4 Connecting thin-layer structures to overall scales

The model proposed here for high Reynolds number turbulence flow fields is consistent with numerical simulations and experiments, and shows how the inertial and viscous range statistics can be explained physically by considering the significant

thin layer coherent structures and the weaker random fluctuations that lie between them. These thin layer structures usually lie within larger structures that may span the whole flow over a scale Λ. Observations and numerical simulations (e.g. of mixing layers and buoyant plumes) indicate that inertial instabilities and non-linear distortions, lead to smaller and quasi-independent structures of decreasing scale $L_1, L_2, ..., L_m$, where $L_1 \sim \Lambda$ and so on until for $m = M_s$, $L_m = L$, which is also of order L_S, the distance between thin layer structures, shown in Fig. 7. The ratio of L_m to L_{m+1} is significantly greater than unity typically $\beta \sim 5$ (e.g. eddies in boundary layers and convective turbulence) (Fig. 7).

But the inertial range process only occurs over scales less than L (which is of order $\Lambda\beta^{-M_s}$ if there is an approximately self similar reduction (by a factor $\beta > 1$) in the scales of the large scale structures). From simulation and experiments, the minimum value of the Reynolds number, Re^*, for the eddies between thin layers to have a fully developed inertial range structure is $Re^* \sim 10^5$. Therefore the minimum value of the macroscale Reynolds number Re_Λ for inertial range turbulence to exist is

$$Re_\Lambda = u_o \Lambda/\nu \gtrsim \beta^{M_s} Re^* \quad \text{or} \quad M_s \lesssim \frac{\ln(Re_\Lambda/Re^*)}{\ln(\beta)}.$$

For the large scale eddies in typical geophysical flows (where $Re_\Lambda \sim 10^{11}$), the number of generations M_s of sub-structures is seldom greater than about 3–5. In the simulations (IKH) and experiments (Section 2; [51]), $M_s \sim 1$. In mixing layers $M_s \sim 3$ [89]. This low number of M_s means that the inertial range covers most of the turbulent energy. But in atmospheric flows it is found that the inertial range spectrum is only valid for $k \geq \Lambda/100$ i.e. $M_s \sim 2$–3 (e.g. [42, 90]).

The mechanisms proposed in the model, and the conditional results of IKH, show how in the vicinity of significant thin shear layers there is a spatial ordering of larger and smaller eddy motions depending on the distance from the thin layer. Also the smaller scales are shielded from larger scales. Therefore the inertial range spectrum is only generally valid over scales of order L_S. These small scale interactions and the blocking action at the interface deflects eddies into different directions as well as the tendency of distorted shear layers to roll up, tend to make the small scale turbulence near the thin layers less anisotropic. However if the large scales are highly anisotropic and non-Gaussian, as with buoyant convection [91], the distribution of thin layers are likely to be anisotropic, which also affects higher order statistics [43].

The sheltering effect of the shear layers implies that the typical distance L_S between the thin layers (see Fig. 8) is of the order of the scale L of the large eddies impacting on the layers in typical conditions (without rapid changes or extraneous influences). The models shows that a quasi-universal eddy structure forms with an average transfer of energy per unit volume $\langle\epsilon\rangle \sim {u_o}^3/L$ towards the significant thin layers, where viscous dissipation ensures the local equilibrium, like waves breaking on a beach. The model implies therefore that L is in fact equivalent to the 'dissipation integral' length scale, L_ϵ that defines the energy transfer process i.e. $L_\epsilon \sim L \sim {u_o}^3/\langle\epsilon\rangle$. In general L_ϵ is not a constant fraction of the overall integral scale of the flow Λ, because of the intermediate generations of eddy structure between these two lengths [92]. For example in anisotropic boundary layer flows Λ defines large eddies, while L_ϵ defines the scale below which there is an inertial range spectrum. Observations show how this is the length scale of typical sheared structures near the ground (e.g. [88]).

4 Conclusions and Discussion

4.1 Structure of significant thin layers in homogeneous turbulence

The main conclusion from our study of the local and overall statistics of fully developed homogeneous turbulence in IKH, the laboratory experiments of Worth and Nickels [51] described in Section 2, is that in these high Re flows there are two characteristic regions associated with the significant thin layers (defined within the smallest integral scales where energy is introduced). The thickness of these layers ℓ is of the order of the Taylor microscale which occupy a small part of the volume of the order of $10{R_\lambda}^{-1}$. Outside the layers the turbulence is distorted, which leads to intense micro scale vortices being generated within the layers. The maximum velocity fluctuations of the vortices are of the order of u_o the energy containing eddies. The thickness of the microscale vortices is the same as in the KO model, namely $\ell/{R_\lambda}^{1/2}$. Their lengths are of order $L/{R_\lambda}^{1/2}$. Away from the significant layers, there are regions of quasi-homogeneous and quasi-isotropic turbulence with smaller amplitude microscale fluctuations, which broadly correspond to the KO model of homogeneous turbulence.

In IKH it is shown that the total volume of the significant thin layers is small, so that they do not contribute significantly to low order statistics (e.g. variance, mean dissipation). However, it is expected that they may dominate the extreme point values of the statistical distributions of dissipation, velocity and vorticity fluctuations, so that they are the key to understanding the nature of strong intermittency (high order statistics) in high Reynolds number turbulence. It would be interesting to examine this idea. It is left for future study.

It is important to realize that other small-scale, lower intensity intermittent structures exist between the significant thin layers, as experiments using flow visualization (Section 2) and statistical wavelet methods [24] both indicate. The net contribution of all these structures to energy spectra is greater than that of the significant thin layer structures, where the greatest dissipation and enstrophy occur.

From the basic statistics of the overall flow, i.e. spectra and correlations to second and third order, it is not possible to distinguish between these two characteristic regions. The simulations and modelling presented here have shown that outside the 'significant' thin layers the spectra have the same form as in the inertial range of the KO theory. Inside the layers they have the same form as for the viscous range of KO theory. (It is a well-known result of spectral analysis that similar forms are found for different kinds of signal, e.g. [57].) The wavelet analysis by Argoul et al. [24] of their measurements of homogeneous turbulence also suggest that the different ranges of the spectra (for the whole flow) are systematically separated in space, which is consistent with our finding.

However, it is expected that the different regions produce relatively different contributions to the fourth and higher order statistics. This has yet to be investigated. As in other turbulent flows with different types of coherent and non-coherent regions the distinct flow features and local statistics of the coherent thin layer regions have been identified through analysing the conditional statistics. Combining this data with our idealised model of vortical interactions between large and small-scale fluctuations leads to a description of the characteristic dynamical mechanisms near and within the thin layers.

The significant thin layers influence the much larger scale motions outside them because their intense mean vorticity (greater than that of the large scales) can adjust so as to shelter or block the outer motions. Through distorting smaller scales these larger scale motions induce both down scale and upscale transfer of energy outside the thin layers [40]. These net downscale motions, that are highly inhomogeneous on a local-scale—like waves being absorbed at critical layers or on beaches—determine the characteristic structures with greatest persistence which, as shown in IKH, defines the form of their inertial range energy spectrum, given by Eq. 15d. But since the thin layers occupy a small part of the flow, the dominant contribution to the inertial subrange and non-linear transfer of energy over the whole flow is determined by local eddy structures in the regions between the thin layers (see IKH and Section 2). These local structures with a quasi-homogeneous distribution have lower strain and vorticity than in the significant layers and are consistent with the estimates of eddy structure derived from KO theory (e.g. [24, 25]).

The spatial flux of external energy towards the layers transfers energy into the thin layers, where intense elongated microscale vortices are induced close to each other, leading to the energy dissipation being much greater than in the quasi-homogeneous regions. It appears that as the vortices grow they are shielded within the shear layer (e.g. [69]) so that they can exist over much longer periods (greater than a characteristic 'turn-over' time) as has often been noted in experiments. Their velocity is of the order of the mean velocity jump across the layer-the maximum possible value without the layer being disrupted. The jump velocity is also comparable to the rms velocity.

The intermittency of intense gradients and dissipation in these layers associated with the distinct vortex structures define the higher order statistics. (They also define higher moments of velocity differences, but this will be considered in a later paper.)

4.2 Implications and uncertainties of the model

The proposed structure for the eddy motions of homogeneous turbulence has implications for how the turbulence develops in time and space. Where the flows that lead to the initial generation of eddy motions include thin layers at high Reynolds number, e.g. by sharp edges of static or moving rigid surfaces, such as plates or bars or aerofoils, they immediately block the larger eddies and generate small scales, even when the Taylor microscale Reynolds number is only about 100 [9, 93]. This is a faster process (being of order of T_L) than by large-scale eddy-eddy distortion mechanisms which take times greater than T_L [73]. In other words the thin layers are an important catalyst for the fast generation of the small-scale structure. These layers also shield the smaller scale eddy motions from those with scales greater than L, which have characteristic non-universal features and depending on how the flow was generated. In general they are anisotropic and unsteady. Thus the smaller eddy motions recirculate within the protected spaces between the layers and eventually become isotropic, as is observed even in flows where the large scales are highly inhomogeneous, and anisotropic (see IKH, and [57]).

At large scales, the shielding effect of vortex structures can reduce long range correlations, which has been suggested as analogous to the 'Debye' shielding in electrostatics, first by Ruelle [94] and later by Ishida et al. [95] and Davidson [96]. The shielding mechanism provides a physical explanation for why there is a sudden

transition in the energy spectra of inhomogeneous and anisotropic turbulent flows at high Reynolds number at a wavenumber k^* (e.g. as reviewed by Hunt and Vassilicos [57] and Wyngaard [42]). In such flows both the quasi-universal eddy structure on scales smaller than the typical distance $L^* \sim k^{*-1}$, are shielded by the layers from the non-universal forms of the large scale eddy motions. There is a sharper transition for the spectrum than in statistical physics models, based on the gradual transitions between the larger eddy straining motions that are non-universal (e.g. shear) and the smaller scale motions associated with the cascade process (e.g. [97]).

In many complex flows, as flow visualization studies have demonstrated, the thin-shear layers in some flows are disrupted, e.g. by strong turbulence outside shear layers [98], while in other flows they can be strengthened and orientated preferentially by the non-universal and anisotropic larger scale motions, e.g. shear or stable stratification. This is a further reason for the common observation for the marked variation in the sharpness of the transitions in energy spectra between anisotropic non-universal large-scale forms to their more universal small scale form in the inertial subrange (e.g. [57]).

More detailed conditional measurements, local simulations (e.g. [71]) and theoretical modelling of these local, quasi-deterministic mechanisms are needed to improve understanding of these transition processes. They would assist the development of simulation methods, such as Large Eddy Simulations, local statistical models and modelling of practical applications—see below.

4.3 Turbulence structure revealed by applications

Studying applications often helps reveal fundamental aspects of scientific phenomena, and this is the case with the structure of high Reynolds number turbulence.

For example, solving practical problems in engineering and environmental flows usually requires understanding the characteristic features of turbulence in space and time. Quantitative models are also needed both for relevant aspects of the flow fields and for 'associated' processes depending on the application, such as the advection and diffusion of scalars, or the motions of particles and bubbles that depend on the acceleration and velocity fields.

In many flows the associated processes are most significant within and near the coherent structures, for example leading to bubbles concentrating in vortices, which shows the thin layer microstructure [99] and how with greater concentrations the coherent structures can be reinforced or destroyed [100].

Modelling turbulent flow processes depends greatly on whether the flows and the associated processes are or are not close to a statistically steady state, which generally depends on whether the associated process are also dissipative. This can occur in fluctuating homogeneous scalar fields with finite molecular diffusivity [93], and when small particles, which have finite drag, are distributed homogeneously in mixing vessels. But there are also important applications where the processes are not in equilibrium and are inhomogeneous such as dispersion and interactions of marked fluid particles or non-fluid particles released from localised sources in the environment (e.g. [101]).

Both kinds of process can reveal particular aspects of the turbulent structures and their statistics in homogenous turbulence. Consider where the passive scalar fields, e.g. concentrations, with molecular diffusivity D are introduced into homogeneous

turbulence the flow, where the Peclet number $Pe = u_o L/D \gg 1$ is of the order of Re. The distribution of scalars depends on the ratio of their initial scalar integral length scale L_θ to that of the typical distance L between the layers. If L_θ/L is greater than $O(1)$ the significant scalar structures studied in this paper act to produce significant jumps in temperature across the thin layers [93],—which also occurs if the initial scalar field is simply a mean scalar gradient.

This coincidence of temperature and velocity interfaces with significant discontinuities across them was seen clearly in the DNS simulations of such interfaces by Bisset et al. [10] for a turbulent wake boundary and experimentally for a jet boundary by Westerweel et al. [8]. The thickness was of the order of the Taylor microscale as in homogeneous turbulence. These are both flows with inhomogeneous turbulence and scalar fluctuations, showing that the formation of sharp interfaces with significant shear is a robust process. If L_θ is initially less than $O(L)$ the role of the thin shear layers is initially less significant for the scalar field, but over time the scalar spectrum follows the spectrum of the velocity over the inertial range.

Within the thin shear layers, whatever the ratio of L_θ/L, viscous and molecular diffusion are significant. The new structure identified here for the significant thin shear layers may affect current models of scalar mixing that are based on particular models of the turbulence microstructure (e.g. [102]).

If the molecular diffusivity is several orders of magnitude less than that of the molecular kinematic viscosity, the scalar microstructure does not develop on the time scale of the thin shear layers. Then the larger scale spectrum for the scalar is affected, with important implications for oceanic and perhaps astrophysical flows [103].

Acknowledgements This paper greatly benefited from discussions at the Isaac Newton Institute Workshop in 2008 and at the Kavli Institute for Theoretical Physics in 2011. Professor G.I. Barenblatt, H. K. Moffatt, and Z. Warhaft helped us understand this model better and its historical context. Professor Sreenivasan clarified our thinking about cascades. JCRH is grateful for being invited to give an early version of the theoretical ideas in this paper [104] at Hong Kong University of Science and Technology in Dec 2009, as well as to support from Arizona State University, Notre Dame University, HongKong University, T.U.Delft. JCRH has been supported by Qinetiq and Atlas Elektronik for turbulence structure studies. Travel funds for visiting Nagoya were provided by Trinity College Cambridge. Support for JCRH by NERC Centre for Polar observation and Modelling at UCL is gratefully acknowledged. The computations were carried out on the Earth Simulator at Japan Agency for Marine-Earth Science and Technology and on the Fx1 system at the Information Technology Center of Nagoya University. This work was partly supported by Grant-in-Aids for Scientific Research (C)23540447 and (C)23560194, from the Japan Society for the Promotion of Science, and also by JST, CREST.

References

1. Ishihara, T., Gotoh, T., Kaneda, Y.: Study of high-reynolds number isotropic turbulence by direct numerical simulation. Annu. Rev. Fluid Mech. **41**, 165–180 (2009)
2. Ishihara, T., Kaneda, Y., Hunt, J.C.R.: Thin shear layers in high Reynolds number turbulence—DNS results (2013). doi:10.1007/s10494-013-9499-z
3. Kolmogorov, A.N.: The local structure of turbulence in incompressible viscous fluid for very large reynolds number. C. R. Acad. Sci. URSS **30**, 299–303 (1941)
4. Obukhov, A.M.: Spectral energy distribution in a turbulent flow. Dokl. Akad. Nauk SSSR **32**, 22–24 (1941)
5. Cadot, O., Douady, S., Couder, Y.: Characterization of the low-pressure filaments in a three-dimensional turbulent shear flow. Phys. Fluids **7**(3), 630–646 (1995)

6. Voth, G.A., Porta, A.L., Crawford, A.M., Alexander, J., Bodenschatz, E.: Measurement of particle accelerations in fully developed turbulence. J. Fluid Mech. **469**, 121–160 (2002)
7. Porta, A.L., Voth, G.A., Moisy, F., Bodenschatz, E.: Using cavitation to measure statistics of low-pressure events in large-reynolds-number turbulence. Phys. Fluids **12**, 1485–1496 (2000)
8. Westerweel, J., Fukushima, C., Pedersen, J.M., Hunt, J.C.R.: Momentum and scalar transport at the turbulent/non-turbulent interface of a jet. J. Fluid Mech. **631**, 199–230 (2009)
9. Braza, M., Perrina, R., Hoarau, Y.: Turbulence properties in the cylinder wake at high reynolds numbers. J. Fluids Struct. **22**, 757–771 (2006)
10. Bisset, D.K., Hunt, J.C.R., Rogers, M.M.: The turbulent/non-turbulent interface bounding a far wake. J. Fluid Mech. **451**, 383–410 (2002)
11. Ganapathisubramani, B., Lakshminarasimhan, K., Clemens, N.T.: Investigation of three-dimensional structure of fine scales in a turbulent jet by using cinematographic stereoscopic particle image velocimetry. J. Fluid Mech. **598**, 141–175 (2008)
12. Moisy, F., Jiménez, J.: Geometry and clustering of intense structures in isotropic turbulence. J. Fluid Mech. **513**, 111–133 (2004)
13. Ruetsch, G., Maxey, M.: The evolution of small-scale structures in homogeneous isotropic turbulence. Phys. Fluids A **4**, 2747–2766 (1992)
14. Dritschel, D.G., Haynes, P.H., Juckes, M.N., Shepherd, T.G.: The stability of a two-dimensional vorticity filament under uniform strain. J. Fluid Mech. **230**, 647–665 (1991)
15. Hunt, J., Eames, I., Westerweel, J.: Vortical interactions with interfacial shear layers. In: Kaneda, Y. (ed.) Proceedings of IUTAM Conference on Computational Physics and New Perspectives in Turbulence, pp. 331–338. Springer (2008)
16. Townsend, A.A.: The Structure of Turbulent Shear Flow. Cambridge University Press (1976)
17. Kida, S., Hunt, J.: Interaction between different scales of turbulence over short times. J. Fluid Mech. **201**, 411–445 (1989)
18. Hussain, A.K.M.F., Reynolds, W.C.: The mechanics of an organized wave in turbulent shear flow. J. Fluid Mech. **41**(2), 241–258 (1970)
19. Hunt, J.C.R., Durbin, P.A.: Perturbed vortical layers and shear sheltering. Fluid Dyn. Res. **24**, 375–404 (1999)
20. Hunt, J.: Turbulence structure in thermal convection and shear-free boundary layers. J. Fluid Mech. **138**, 161–184 (1984)
21. Hunt, J.: A theory of turbulent flow round two-dimensional bluff bodies. J. Fluid Mech. **61**(4), 625–706 (1973)
22. Lundgren, T.: Strained spiral vortex model for turbulent fine structure. Phys. Fluids **25**, 21–93 (1982)
23. Horiuti, K., Ozawa, T.: Multi-mode stretched spiral vortex and nonequilibrium energy spectrum in homogeneous shear flow turbulence. Phys. Fluids **23**, 035107 (2011)
24. Argoul, F., Arneodo, A., Grasseau, G., Gagne, Y., Hopfinger, E.J., Frisch, U.: Wavelet analysis of turbulence reveals the multifractal nature of the richardson cascade. Nature **338**, 51–53 (1989)
25. Elsinga, G.E., Marusic, I.: Universal aspects of small-scale motions in turbulence. J. Fluid Mech. **662**, 514–539 (2010)
26. Richardson, L.F.: Weather Prediction by Numerical Process. Cambridge University Press (1922)
27. Richardson, L.F.: Atmospheric diffusion shown on a distance-neighbour graph. Proc. R. Soc. Lond. A **110**, 709–737 (1926)
28. Jones, J.G., Watson, G.H., Foster, G.W.: Non-gaussian statistics of atmospheric turbulence and related effects on aircraft loads. AIAA J. **42**, 2438–2447 (2004)
29. Tsinober, A.: Vortex stretching versus production of strain/dissipation. In: Hunt, J.C.R., Vassilicos, J.C. (eds.) Proc. Conf at INI. Cambridge on Vortex Dynamics and Turbulence, pp. 164–191. Cambridge University Press (2000)
30. Corrsin, S., Kistler, A.: Free-stream boundaries of turbulent flows. NACA Tech. Rep. 1244, pp. 1033–1064 (1955)
31. Holzner, M., Liberzon, A., Nilkitin, N., Luhti, B., Kinzelbach, W., Tsinober, A.: Small-scale aspects of flows in proximity of the turbulent/nonturbulent interface. Phys. Fluids **19**, 71702 (2007)
32. Holmes, P., Lumley, J.L., Berkooz, G.: Turbulence, Coherent Structures, Dynamical Systems and Symmetry. Cambridge University Press (1996)
33. Hussain, A.K.M.F.: Coherent structures and turbulence. J. Fluid Mech. **173**, 303–356 (1986)
34. Bonnet, J.P., Glauser, M.N.: Eddy Structure Identification in Free Turbulent Shear Flows. Kluwer Academic Press (1993)

35. Hunt, J.: Dynamics and statistics of vortical eddies in turbulence. In: Hunt, J.C.R., Vassilicos, J.C. (eds.) Turbulence Structure and Vortex Dynamics, pp. 192–243. Cambridge University Press (2000)
36. Kraichnan, R.H.: On kolmogorov's inertial-range theories. J. Fluid Mech. **62**(2), 305–330 (1974)
37. Mydlarski, L., Pumir, A., Shraiman, B.I., Siggia, E.D., Warhaft, Z.: Structures and multipoint correlators for turbulent advection: Predictions and experiments. Phys. Rev. Lett. **81**, 4373–4376 (1998)
38. Domaradzki, J.A., Liu, W., Brachet, M.E.: An analysis of subgrid-scale interactions in numerically simulated isotropic turbulence. Phys. Fluids A **5**, 1747–1749 (1993)
39. Gotoh, T., Watanabe, T.: Statistics of transfer fluxes of the kinetic energy and scalar variance. J. Turbul. **6**, 1–18 (2005)
40. Aoyama, T., Ishihara, T., Kaneda, Y., Yokokawa, M., Itakura, K., Uno, A.: Statistics of energy transfer in high-resolution direct numerical simulation of turbulence in a periodic box. J. Phys. Soc. Jpn. **74**, 3202–3212 (2005)
41. Ooms, G., Boersma, B., Pourquie, M.: Numerical simulation of the spectral development of inviscid helical flows. Eur. J. Mech. B-Fluids **30**, 428–436 (2011)
42. Wyngaard, J.C.: Turbulence in the Atmosphere. Cambridge University Press (2010)
43. Sreenivasan, K.R.: On local isotropy of passive scalars in turbulent shear flows. Proc. Roy. Soc. A **434**, 165–182 (1991)
44. Zocchi, G., Tabeling, P., Maurer, J., Willaime, H.: Measurement of the scaling of the dissipation at high reynolds numbers. Phys. Rev. E **50**, 3693–3700 (1994)
45. Belin, F., Maurer, J., Tabeling, P., Willaime, H.: Velocity gradient distributions in fully developed turbulence: An experimental study. Phys. Fluids **9**(12), 3843–3850 (1997)
46. Worth, N.A., Nickels, T.B., Swaminathan, N.: A tomographic piv resolution study based on homogeneous isotropic turbulence dns data. Exp. Fluids **49**, 637–656 (2010)
47. Sreenivasan, K.R.: An update on the energy dissipation rate in isotropic turbulence. Phys. Fluids **10**(2), 528–529 (1998)
48. Worth, N.: Tomographic-piv measurement of coherent dissipation scale structures. Ph.D. thesis, University of Cambridge (2010)
49. Sreenivasan, K.R.: On the universality of the kolmogorov constant. Phys. Fluids **7**(11), 2778–2784 (1995)
50. Gotoh, T., Fukayama, D., Nakano, T.: Velocity field statistics in homogeneous steady turbulence obtained using a high-resolution direct numerical simulation. Phys. Fluids **14**(3), 1065–1081 (2002)
51. Worth, N.A., Nickels, T.B.: Some characteristics of thin shear layers in homogeneous turbulent flow. Phil. Trans. R. Soc. A **369**, 709–722 (2011)
52. Miyazaki, T., Hunt, J.: Linear and nonlinear interactions between a columnar vortex and external turbulence. J. Fluid Mech. **402**, 349–378 (2000)
53. Verzicco, R., Jiménez, J., Orlandi, P.: On steady columnar vortices under local compression. J. Fluid Mech. **299**, 367–388 (1995)
54. Frisch, U.: Turbulence: The Legacy of A. N. Kolmogorov. Cambridge University Press, Cambridge (1995)
55. Kevlahan, N., Hunt, J.C.R., Vassilicos, J.C.: A comparison of different analytical techniques for identifying structures in turbulence. Appl. Sci. Res. **53**, 339–355 (1994)
56. Kevlahan, N., Hunt, J.: Nonlinear interactions in turbulence with strong irrotational straining. J. Fluid Mech. **337**, 333–364 (1997)
57. Hunt, J., Vassilicos, J.: Kolmogorov's contributions to the physical and geometrical understanding of small-scale turbulence and recent developments. Proc. Roy. Soc. A **434**, 183–210 (1991)
58. Hunt, J.: Developments in computational modelling of turbulent flows. In: Pironneau, O., Rodi, W., Rhyming, I.L., Savill, A.M., Truong, T.V. (eds.) ERCOFTAC Workshop on Numerical Simulation of Unsteady Flows and Transition to Turbulence, pp. 1–76. Cambridge Univ. Press (1992)
59. George, W.K.: The decay of homogenous isotropic turbulence. Phys. Fluids A **4**, 1492–1509 (1992)
60. Landau, L.D., Lifshitz, E.M.: Fluid Mechanics, 2nd edn. Pergamon Press (1987)
61. Betchov, R.: An inequality concerning the production of vorticity in isotropic turbulence. J. Fluid Mech. **1**, 497–504 (1956)
62. Hunt, J.C.R., Delfos, R., Eames, I., Perkins, R.J.: Vortices, complex flows and inertial particles. Flow Turbulence Combust. **79**(3), 207–234 (2007)

63. Batchelor, G.K., Townsend, A.A.: The nature of turbulent motion at large wave-numbers. Proc. Roy. Soc. London A **199**, 238–255 (1949)
64. Verzicco, R., Jiménez, J.: On the survival of nonuniform vortex filaments in model turbulence. J. Fluid Mech. **394**, 261–279 (1999)
65. Britter, R., Hunt, J., Mumford, J.C.: The distortion of turbulence by a circular cylinder. J. Fluid Mech. **92**(2), 269–301 (1979)
66. Jacobs, R.G., Durbin, P.A.: Shear sheltering and the continuous spectrum of the orrsommerfeld equation. Phys. Fluids **10**(8), 2006–2011 (1998)
67. Chu, C.C., Falco, R.E.: Vortex ring/viscous wall layer interaction model of turbulence production process near walls. Exp. Fluids **6**, 305–315 (1988)
68. Porta, A.L., Voth, G.A., Crawford, A.M., Alexander, J., Bodenschatz, E.: Fluid particle accelerations in fully developed turbulence. Nature **409**, 1017–1019 (2001)
69. Zaki, T., Saha, S.: On shear sheltering and the structure of vortical modes in single- and two-fluid boundary layers. J. Fluid Mech. **626**, 111–147 (2009)
70. Zilitinkevich, S., Hunt, J., Esau, I., Grachev, A., Lalas, D., Akylas, E., Mombrou, M., Fairall, C., Fernando, H.S., Baklanov, A.A., Joffre, S.M.: The influence of large convective eddies on the surface-layer turbulence. Q. J. R. Meteorol. Soc. **132**, 1423–1456 (2006)
71. da Silva, C.B., dos Reis, R.: The role of coherent vortices near the turbulent/nonturbulent interface in a planar jet. Phil. Trans. R. Soc. A **369**, 738–753 (2011)
72. Sadeh, W.Z., Sutera, S., Maeder, P.: An investigation of vorticity amplification in stagnation flow. Z. Angew. Math. Phys. **21**, 717–742 (1970)
73. Hunt, J., Carruthers, D.J.: Rapid distortion theory and the 'problems' of turbulence. J. Fluid Mech. **212**, 497–532 (1990)
74. Farge, M., Hunt, J.C.R., Vassilicos, J.C.: Wavelets, Fractals, and Fourier Transforms. Clarendon Press (1993)
75. Batchelor, G.K.: The Theory of Homogeneous Turbulence. Cambridge University Press, Cambridge (1953)
76. Tennekes, H., Lumley, J.L.: A First Course in Turbulence. The MIT Press (1972)
77. Ishihara, T., Kaneda, Y., Yokokawa, M., Itakura, K., Uno, A.: Small-scale statistics in high-resolution direct numerical simulation of turbulence: Reynolds number dependence of one-point velocity gradient statistics. J. Fluid Mech. **592**, 335–366 (2007)
78. Hunt, J., Moin, P., Lee, M., Moser, R., Spalart, P., Mansour, N., Kaimal, J., Gaynor, E.: Cross correlation and length scales in turbulent flows near surfaces. In: Advances in Turbulence 2 (2nd European Turbulence Conf., Berlin, August 1988), pp. 128–134. Springer-Verlag (1989)
79. Mann, J.: The spatial structure of neutral atmospheric surface-layer turbulence. J. Fluid Mech. **273**, 141–168 (1994)
80. Batchelor, G.K.: An Introduction to Fluid Dynamics. Cambridge University Press, Cambridge (1967)
81. Bourguet, R., Braza, M., Perrin, R., Harran, G.: Anisotropic eddy-viscosity concept for strongly detached unsteady flows. AIAA J. **45**, 1145–1149 (2007)
82. Wu, X., Jacobs, R., Hunt, J., Durbin, P.A.: Simulation of boundary layer transition induced by periodically passing wakes. J. Fluid Mech. **398**, 109–153 (1999)
83. Lee, M.J., Kim, J., Moin, P.: Structure of turbulence at high shear rate. J. Fluid Mech. **216**, 561–583 (1990)
84. Savill, A.M.: Recent developments in rapid-distortion theory. Annu. Rev. Fluid Mech. **19**, 531–575 (1987)
85. Hanazaki, H., Hunt, J.: Structure of unsteady stably stratified turbulence with mean shear. J. Fluid Mech. **507**, 1–42 (2004)
86. She, Z.S., Jackson, E.: On the universal form of energy spectra in fully developed turbulence. Phys. Fluids A **5**(7), 1526–1528 (1993)
87. Perry, A.E., Abell, C.J.: Scaling laws for pipe-flow turbulence. J. Fluid Mech. **67**(2), 257–271 (1975)
88. Hogstrom, U., Hunt, J., Smedman, A.S.: Theory and measurements for turbulence spectra and variances in the atmospheric neutral surface layer. Bound.-Layer Meteorol. **103**, 101–124 (2002)
89. Moser, R.D., Rogers, M.M.: Mixing transition and the cascade to small scales in a plane mixing layer. Phys. Fluids A **3**(5), 1128–1134 (1991)
90. Hunt, J.C.R., Phillips, O.M., Williams, D.: Turbulence and stochastic processes: Kolmogorov's ideas 50 years on. Proc. Roy. Soc. London A **434**, 1–240 (1991)
91. Hunt, J., Kaimal, J.C., Gaynor, J.E.: Eddy structure in the convective boundary layer–new measurements and new concepts. Q. J. R. Meteorol. Soc. **114**, 827–858 (1988)

92. Mazzi, B., Vassilicos, J.C.: Fractal-generated turbulence. J. Fluid Mech. **502**, 65–87 (2004)
93. Warhaft, Z.: Passive scalars in turbulent flows. Ann. Rev. Fluid Mech. **32**, 203–240 (2000)
94. Ruelle, D.: Is there screening in turbulence? J. Stat. Phys. **61**, 865–868 (1990)
95. Ishida, T., Davidson, P.A., Kaneda, Y.: On the decay of isotropic turbulence. J. Fluid Mech. **564**, 455–475 (2006)
96. Davidson, P.A.: Long-range interactions in turbulence and the energy decay problem. Phil. Trans. R. Soc. A **369**, 796–810 (2011)
97. Hunt, J., Sandham, N., Vassilicos, J., Launder, B., Monkewitz, P., Hewitt, G.: Developments in turbulence research: a review based on the 1999 programme of the Isaac Newton Institute, Cambridge. J. Fluid Mech. **436**, 353–391 (2001)
98. Hancock, P.E., Bradshaw, P.: Turbulence structure of a boundary layer beneath a turbulent free stream. J. Fluid Mech. **205**, 45–76 (1989)
99. Douady, S., Couder, Y., Brachet, M.E.: Direct observation of the intermitency of intense vorticity filaments. Phys. Rev. Lett. **67**, 983–986 (1991)
100. Sene, K.J., Thomas, N.H., Hunt, J.C.R.: The role of coherent structures in bubble transport by turbulent shear flows. J. Fluid Mech. **259**, 219–240 (1994)
101. Hunt, J.: Turbulent diffusion from sources in complex flows. Annu. Rev. Fluid Mech. **17**, 447–485 (1985)
102. Batchelor, G.K.: Small-scale variation of convected quantities like temperature in turbulent fluid. Part 1. General discussion and the case of small conductivity. J. Fluid Mech. **5**, 113–133 (1959)
103. Gibson, C.H.: Kolmogorov similarity hypotheses for scalar fields: Sampling intermittent turbulent mixing in the ocean and galaxy. Proc. Roy. Soc. London A **434**, 149–164 (1991)
104. Hunt, J., Eames, I., Westerweel, J., Davidson, P.A., Voropayev, S., Fernando, J., Braza, M.: Thin shear layers - the key to turbulence structure? J. Hydro Environ. Res. **4**, 75–82 (2010)